Locus coeruleus activity fluctuations set a non-reducible timeframe for mammalian NREM-REM sleep cycles

Alejandro Osorio-Forero[1,2], Georgios Foustoukos[1], Romain Cardis[1], Najma Cherrad, Christiane Devenoges, Laura M.J. Fernandez and Anita Lüthi

Department of Fundamental Neurosciences, University of Lausanne, Rue du Bugnon 9, CH-1005 Lausanne, Switzerland

[1] Equal contribution

[2] Department of Sleep and Cognition. Netherlands Institute for Neuroscience, Meibergdreef 47, 1105 BA Amsterdam, The Netherlands

Correspondence: anita.luthi@unil.ch

Author contributions: AOF, RC and NC, LF and AL originally started this project. GF developed all LC fiber photometry experimentation and corresponding analyses. RC developed the REMS restriction approach. AOF and GF developed analysis scripts, and all authors contributed to data analysis. LF made the final figure versions and schemes. AL wrote the first version of the manuscript, with input from all authors.

Acknowledgements: The authors acknowledge fruitful discussions with Paul Franken, Stephany Fulda, Markus Schmidt, Francesca Siclari, Aurélie Stephan, Mehdi Tafti and Eus van Someren. We thank Dr. Simone Astori and Olivia Zanoletti from the Carmen Sandi lab for carrying out the corticosterone measurements and Aurélie Guillaume-Gentil for assistance with viral injections. The constructive comments of Lila Banterle and Paola Milanese on earlier versions of the manuscript are very appreciated. We are grateful to the animal caretakers, especially Michelle Blom and Titouan Tromme, and to Dr. Laure Sériot for expert veterinary advice. This work was supported by the Swiss National Science Foundation (Grant no. 184759 to AL) and Etat de Vaud.

Conflict of interest. The authors declare no conflict of interest.

Abstract

The noradrenergic *locus coeruleus* (LC) supports vital brain functions during wakefulness. In contrast, the LC has been associated with sleep-promotion and -disruption, leaving its functions for sleep uncertain. Here, we show that the LC is essential for the progression of natural, undisturbed sleep because it creates a non-reducible timeframe for the non-rapid-eye-movement (NREM) sleep-REM sleep cycle. Fiber-photometric jGCaMP8s-based LC activity measures, closed-loop optogenetics and mouse sleep-wake monitoring revealed that LC showed ~50-s-activity fluctuations, during which high activity levels promoted a NREMS with high arousability, while low levels a NREMS with the opportunity for transitions to REMS. The NREMS-REMS cycle was shortened by LC inhibition due to precocious REMS onset. Supporting LC's pivotal role as a gatekeeper of the NREMS-REMS cycle, REMS entries occurred on intervals no shorter than ~50 s during REMS-restriction. A stimulus-enriched wake experience strengthened LC fluctuations, which contributed to subsequent NREMS fragmentation and delayed REMS. The LC fluctuations are hence indispensable for the NREMS-REMS cycle but they can become sleep-disruptive as a result of prior wake experience.

Key words: ultradian sleep cycle || arousability || sleep homeostasis || REMS restriction || automated REMS deprivation || microarousal ||noradrenaline ||norepinephrine || infraslow time scale || optogenetics || K-complex || sleep disorders

Introduction

The pontine brainstem *locus coeruleus* (LC) is a wake-promoting brain area that constitutes the principal source of noradrenaline (NA) for forebrain circuits and alertness-modulating nuclei[1]. LC neuronal activity levels grade with the level of wakefulness[2] and with physiological signatures of cortical[3] and autonomic arousal[4,5], while sleep-promoting brain areas are inhibited[6,7]. Elevated LC activity is implicated in the cognitive and autonomic manifestations of states of hyperarousal during stress- and anxiety-provoking experiences[1,8]. Conversely, clinically important sedatives inhibit LC[9]. Together, this illustrates LC's broad implication in many graduations of states of wakefulness.

The NA-synthetizing LC neurons remain active in sleep[7,10] and elevate arousability[11-13]. During non-rapid-eye-movement sleep (NREMS) in mouse, LC activity fluctuates on an infraslow time scale (30 – 50 s, 0.02 Hz) and generates variations in the levels of free NA, as shown for sensory thalamus and prefrontal cortex[11,12]. NA depolarizes thalamic neurons which leads to a suppression of sleep spindles, an EEG hallmark of NREMS [14], and spindles reappear when NA levels are low[11]. Low spindle density and high LC activity coincide with elevated auditory and somatosensory arousability[13,15,16], in line with LC's wake-promoting effects. Spontaneous arousals that are typical for mammalian NREMS also coincide with moments of low spindle (and thus high LC) activity[12,15].

Activation of NA-synthetizing LC neurons can increase the time spent in NREMS while reducing REMS[11,12,17]. Sleep-active LC neurons could hence disrupt sleep by interfering with its natural progression in NREMS-REMS cycles. Alternatively, LC's natural activity patterns could be relevant for the timing of REMS in natural, undisturbed sleep. Widely used sedatives that interfere with NA signaling also modify REMS in humans[18,19]. Therefore, a balanced assessment of LC's REMS-regulatory and REMS-disruptive actions is desirable. Also, a precocious onset of REMS at the beginning of the night is important in the diagnosis of psychiatric disorders, and a successful monoaminergic antidepressant treatment restores REMS timing[20]. Recent functional imaging studies in humans indicate that LC function during wake associates negatively with REMS quality[21]. Examining natural LC activity's role in sleep architecture is hence pressing as its implication in human sleep becomes increasingly recognized.

Here, we show that both, the arousability-regulating and REMS-suppressing roles of LC, are integral to natural, undisturbed sleep, but they are temporally segregated. When LC activity fluctuations reached high levels, NREMS was promoted and spontaneous arousals occurred preferentially, while low levels allowed entries into REMS. We found that LC activity fluctuations imposed a minimal time to be spent in NREMS before allowing REMS, thus being of fundamental importance in the temporal composition of the natural NREMS-REMS cycles. The strength of LC activity

fluctuations in NREMS increased when preceded by a stimulus-enriched wake experience, causing more arousals and delaying REMS. Together, we identify a neural mechanism that is a gatekeeper for mammalian sleep's natural progression but that can become disruptive if modified by preceding wake experience.

Results

Noradrenergic LC neuronal activity levels varied characteristically across wake, NREMS and REMS

To monitor the activity of LC neurons during unperturbed sleep, we conditionally expressed the genetically encoded Ca^{2+} sensor jGCaMP8s in dopamine-β-hydroxylase-(DBH)-Cre mice, previously shown to drive the expression of viral constructs in NA-synthetizing neurons with a high degree of specificity (> 80 %)[11]. jGCaMP8s is the latest variant of the circular green fluorescent protein (GFP) -based Ca^{2+} sensors that responds to neuronal activity-induced intracellular Ca^{2+} elevations with millisecond resolution and high dynamic range[22]. We then implanted animals with EEG/EMG electrodes for sleep and an optic fiber stub over the LC for fiber photometric recordings (**Fig. 1a, b**). Additionally, local field potential (LFP) electrodes were implanted in the primary somatosensory S1 cortex and in the hippocampal CA1 areas. The EEG signals served to score the major vigilance states Wake, NREMS and REMS and the microarousals (MAs) based on standard polysomnography. The S1 LFP recordings were used to monitor the dynamics of power bands characteristic for NREMS and the CA1 LFP recordings to define the onset of REMS (see Methods).

Across the 12-h light phase, the major resting phase of mice, the photometrically recorded Ca^{2+} activity of noradrenergic LC populations ('LC activity') varied characteristically with states of wake, NREM and REMS, consistent with recent studies (**Fig. 1c**)[12,17]. LC activity was tonically elevated during wakefulness, but it declined in NREMS to a lower baseline on top of which a fluctuating pattern appeared. In 8 animals with a dynamic range of relative fluorescence changes of 16.3 – 95.3 % in the first 2 h of recordings (mean 44.8 ± 11.8 %) and a histologically confirmed fiber positioning (**see Fig. 1b**), LC fluctuations continued throughout much of the NREMS bouts and occasionally coincided with MAs (**Fig. 1c**). With REMS onset, LC activity fluctuations ceased but resumed once REMS and a subsequent brief subsequent arousal ended and NREMS restarted. Mean LC activity levels, calculated for the first 2 h of the resting phase, were significantly different between the three vigilance states (**Fig. 1d**) (for detailed statistics here and in all following figure panels, see **Suppl. Table 1**). The fluctuations generated time-locked variations in free NA levels, as verified through dual fiber photometric measures of LC activity and fluorescence of the NA biosensor $GRAB_{NE1h}$[23] expressed in primary somatosensory thalamus (**Fig. 1e**).

LC activity patterns showed a distinct transitional period between wake and NREMS. At NREMS onset that followed wakefulness (> 60 s), baseline LC activity declined with an approximately monoexponential time course (time constant τ = 125.4 ± 18.0 s, n = 8) from the levels of tonic wakefulness to a lower baseline (**Fig. 1f, g**). Over this transitional time period, the frequency of LC activity peaks, detected based on a prominence of > 40% (See Methods and **Suppl. Fig. 1**), declined from 0.24 ± 0.006 Hz to 0.15 ± 0.009 Hz (**Fig. 1h**). These measures are within the range of LC multi-unit discharges during NREMS in rodents[13,24,25].

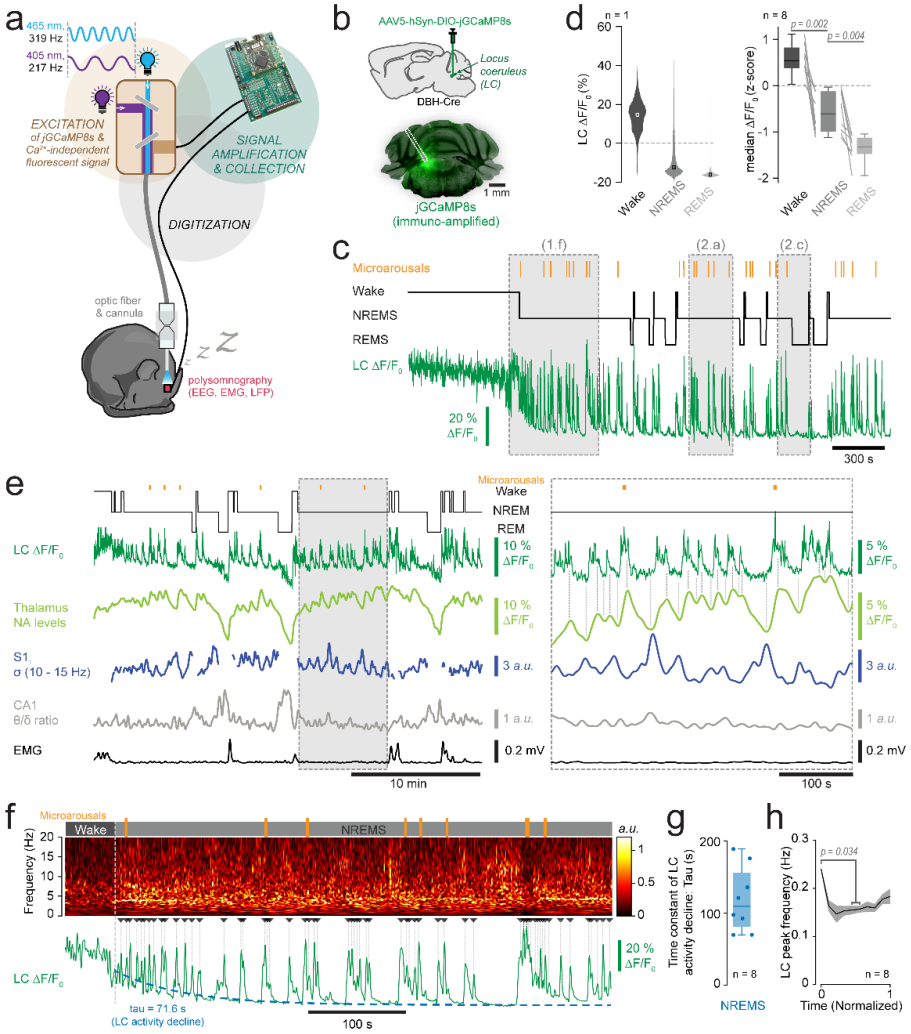

Figure 1. *Locus coeruleus* (LC) activity patterns across wakefulness, NREMS and REMS

a) Experimental scheme for sleep recordings in combination with fiber photometry.

b) Schematic of viral injection into a dopamine-β-hydroxylase-Cre mouse prior to sleep/fiber photometric implantations and example *post hoc* histological verification of jGCaMP8s-GFP expression and optic fiber location.

c) Example sleep hypnogram (black) and jGCaMP8s fluorescent signal (green) recorded from LC (in $\Delta F/F_0$). Orange vertical lines: microarousals (MAs). Grey rectangles: trace portions that are expanded in other figure panels (as indicated).

d) Left, Violin plot of LC fluorescence datapoints for the recording shown in c between ZT0-ZT2; Right, Median z-scored fluorescence for all animals included. One-way repeated-measures ANOVA with *post hoc* t-tests.

e) Example dual fiber photometric recording from an animal that expresses jGCaMP8s in LC and $GRAB_{NE1h}$ in somatosensory thalamus. From top. Hypnogram (black), LC-jGCaMP8s and free NA-$GRAB_{NE1h}$ fluorescence, S1 LFP sigma (σ, 10 – 15 Hz) power, CA1 local field potential (LFP) theta/delta (θ/δ) ratio and absolute EMG levels. Grey rectangle: portion of trace expanded on the right. Vertical lines: coordinated high and low levels of fluorescence signals. Note the coincidence of high LC activity/high NA levels with MAs.

f) Example LC fluorescence signal at a Wake-to-NREMS transition, expanded from c. Time-frequency plot is shown for 0-20 Hz. Dotted blue line: mono-exponential fit of baseline decay, with decay time constant (τ) indicated. Black triangles: automatically detected individual LC fluorescence peaks.

g) Box-and-whisker plot for τ values.

h) Time course of LC fluorescence peak frequency across NREMS bouts normalized in time. Paired t-test.

See Supplementary Table 1 for detailed statistical information.

LC activity fluctuations during NREMS associated with both arousability and REMS onset

We next asked how LC activity fluctuations during NREMS were associated with arousability and the timing of REMS. For arousability, we focused on spontaneous brief MAs that we scored once we noted an EEG desynchronization (commonly defined as a decline of low-frequency combined with the appearance of high-frequency EEG activity) and an EMG activity lasting ≤ 12 s[15,26,27] (see Methods). We determined REMS onset through thresholding the ratio of θ (6 – 10 Hz) / δ (1 – 4 Hz) power in the CA1 LFP.

During consolidated NREMS in the light phase, LC activity peaks co-occurred in 'transients' that were interspaced by periods with low activity. These transients coincided with power declines in the spindle-containing σ (10 – 15 Hz) power band[14], which resurged every time a transient ended (**Fig. 2a1**)[11,12]. During these transients, NREMS either continued or was interrupted by a MA. LC activity transients and σ power were anticorrelated with a time lag of 2.16 ± 0.44 s (n = 8) and showed side peaks at 48.3 ± 2.2 s (**Fig. 2a2**, range 38.5 – 58.1 s, measured in n = 6/8 animals). The LC activity transients thus preceded the spindle-inhibiting effect of LC-dependent NA release[11,28] and occurred on an infraslow time scale (30 – 50 s).

In line with LC's arousal-promoting effect, ~1 out of 3 LC activity transients (30.3 ± 2.9 %, range 15.7 – 40.2 %, n = 8) coincided with a MA within a 5-s time interval. Similar percentages were previously described for the preferential occurrence of MAs with low σ power levels[12,15]. Non-MA-associated transients were smaller than MA-associated ones (**Fig. 2b1**), suggesting that higher LC neuron numbers or activity was required for a MA. However, striking distinctions between non-MA and MA-associated transients became evident when we examined their spectral dynamics using S1 LFP[11] or EEG signals. The non-MA-associated transients showed spectral correlates clearly qualifying them as NREMS- (and not arousal)-promoting (**Fig. 2b2**). There was a remarkable power increase in the NREMS-defining δ frequency band (1.5 – 4 Hz) (n = 7, paired t-test, p = 0.007), whereas wake-related high-frequency γ (60 – 80 Hz) activity decreased (n = 7, paired t-test, p = 0.0001)[29]. During MA-associated transients, these power changes diverged in opposite directions. Here, the δ power increase was suppressed and rapid transients in the wake-related high-frequency γ band appeared. These disruptions were stronger the longer the MA duration, they included other wake-related frequency bands, and they were also present at the level of differential EEG signals (**Suppl. Fig. 2**). The data show that LC activity transients during NREMS were linked primarily to enhanced low-frequency spectral power that is defining continued NREMS. However, a spontaneous MAs secondarily disrupted the low-frequency power increases to let wake-related spectral signatures appear[12,13,15].

The LC activity fluctuations ceased before REMS onset (**Fig. 2c**). Averaging LC activity across all NREMS-to-REMS transitions in the light phase for all 8 animals demonstrated that this decline preceded important markers of REMS onset, in particular an increase in θ (6 – 10 Hz) power and a loss of EMG tone. The transitional phase was further marked by a continued increase in spindle density and σ power levels while LC activity declined, reminiscent of the phase of 'intermediate sleep' that has been described for NREM-to-REMS transitions[14,30-32]. Prolonged LC activity declines, presumably reflecting enhanced inhibitory inputs onto LC[33,34], thus precede transitions from NREM to REMS (hereafter referred to as 'REMS entries').

Together, LC activity in NREMS was linked to arousability control when levels were high and to REMS entries when levels were low. This suggested that LC fluctuations provided a timeframe over which arousals were segregated from sleep's natural progression in NREMS-REMS cycles.

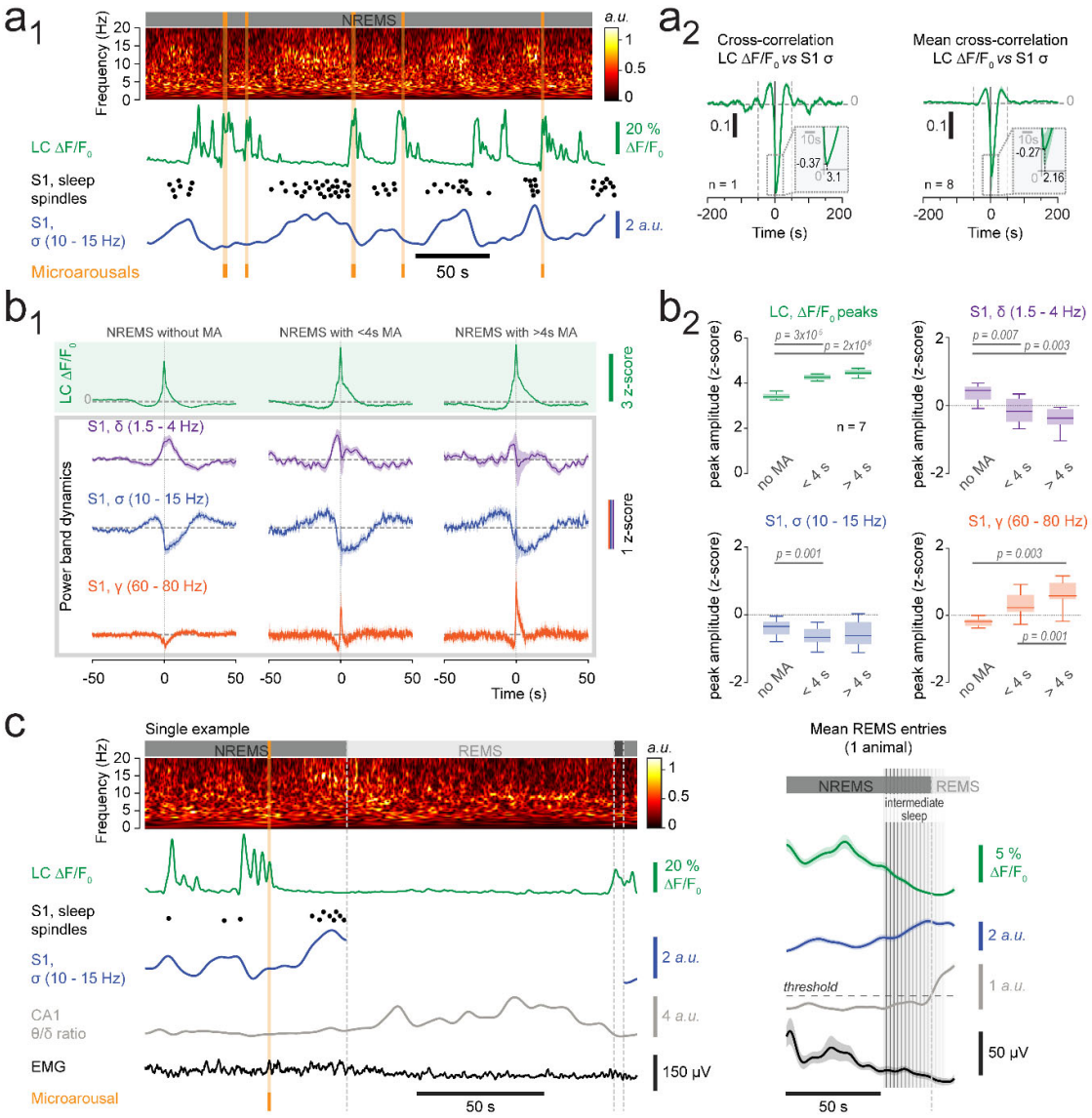

Figure 2. Association of LC activity patterns during NREMS with arousal promotion and REMS entries.

a) a1), Example recording of LC fluorescence during a NREMS bout, expanded from Fig. 1c. Time-frequency plot of S1 LFP from 0 – 20 Hz, S1 σ (10 – 15 Hz) power and individual sleep spindles (black dots) are aligned with LC fluorescent signal. Vertical orange lines: microarousals (MAs); a2), Cross-correlation for LC fluorescence and S1 σ power during NREMS from ZT0-ZT12 and mean cross-correlation across animals. Vertical dotted lines highlight side peaks. Insets; zoom-ins on minima that are complemented with amplitude and lag values.

b) b1) Spectral analysis of S1 LFP signals corresponding to LC fluorescence transients that are classified based on whether they did not or did co-occur with short (< 4 s) or long (> 4 s) MAs. Corresponding power dynamics for the delta (δ), σ and gamma (γ) frequency bands are aligned vertically (grey-lined box); b2) Quantification of mean LC fluorescence and spectral transients between 0 – 5 s. One-way repeated-measures ANOVA followed by *post hoc* t-tests, with Bonferroni correction.

c) Left, Example recording of LC fluorescence during a NREMS-to-REMS transition (expanded from Fig. 1c). Same signals shown as in a, with in addition CA1 θ/δ ratio and EMG. Right, Mean dynamics of these signals for the same animal. Vertical grey lines with shading: presumed period corresponding to 'intermediate sleep'.

See Supplementary Table 1 for detailed statistical information.

LC activity fluctuations segregated arousal control and REMS entries in time during undisturbed NREMS

LC activity fluctuations between high and low levels during NREMS could imply that the control of arousability and of REMS entries takes place in a temporally segregated manner. In this case, REMS entries should not occur when LC is activated at moments when it normally becomes silent. Conversely, these entries should be frequent if LC is inhibited when it normally reaches high levels. To test these possibilities, we optogenetically modified natural LC activity bidirectionally in DBH-Cre animals conditionally expressing either the excitatory opsin channelrhodopsin-2 (ChR2) coupled to the red fluorescent protein mCherry (hChR2(H134R)_mCherry(rev)) or the inhibitory opsin Jaws coupled to enhanced GFP (Jaws_KGC_EGFP) within LC neurons[11]. We tracked LC fluctuations on-line through monitoring the σ power dynamics in the S1 LFP.

To prevent high LC levels from declining, we stimulated LC in ChR2-expressing animals at 1 Hz once σ power was rising (**Fig. 3a**). Stimulations were applied in the first 20 min of every h during ZT1-ZT9, and corresponding sham stimulations (LEDs turned-off) were done in separate sessions[11]. The time spent in REMS and the frequency of REMS entries were reduced during stimulation compared to sham periods, while time spent in NREMS but not wakefulness was increased.

To interrupt elevations of LC activity, we expressed the orange light-activated chloride pump 'Jaws' in DBH-Cre animals to inhibit LC at moments of declining σ activity. To test the efficacy of this inhibition, we studied 2 DBH-Cre animals co-expressing Jaws in the LC and the NA sensor $GRAB_{NE1h}$ in the thalamus. Jaws-inhibition of LC (with continuous light) decreased baseline NA levels in NREMS and partially reduced the decline of NA during REMS, indicating that a subgroup of NA-releasing neurons involved in REMS regulation were inhibited (**Suppl. Fig. 3a**). Jaws-inhibition of LC, applied over the same time intervals as described for ChR2, increased REMS time and the frequency of REMS entries, leaving both NREMS and wake time unaffected (**Fig. 3b**). Therefore, the silencing of natural LC activity was both necessary and sufficient for permitting REMS entries. LC activity fluctuations thus divided mouse NREMS into two functionally distinct periods. When LC activity was high, spontaneous MAs occurred preferentially (see Fig. 2), while REMS entries were prohibited. When LC activity reached low levels, NREMS continued together with the opportunity for REMS entries.

The propensity to enter REMS increases linearly with the time spent in NREMS, which reflects its homeostatic regulation[35]. Furthermore, several REMS-regulating brain areas innervate the LC[34,36-38]. Therefore, LC's REMS-suppressing actions could be weakened in the course of NREMS by a homeostatic downregulation of LC activity fluctuations. Contrary to this possibility, mean LC activity levels across all time-normalized NREMS bouts was stable independently of the length of the NREMS bout and until just prior to REMS onset (**Fig. 3c, d**). The LC fluctuations seemed thus to persist and to gate REMS throughout much of NREMS.

Natural sleep progresses in NREMS-REMS cycles. To start addressing the role of LC in these cycles, we optogenetically inhibited LC in Jaws-expressing DBH-Cre mice at different moments in a NREMS bout. Sessions with light exposure were interleaved with sham sessions. The NREM-REMS cycles in mouse vary in length and architecture[39]. To sample a mostly homogeneous set of NREMS bouts, we focused our experiments on the bouts that were preceded by a relatively long (> 120 s) period of REMS. These begin with a REMS-refractory period, during which REMS entries are unlikely, before the REMS-permissive period starts[39]. When LC inhibition was started during the presumed REMS refractory (Ref) period, we observed no significant change in the frequency of REMS entries or in time spent in REMS compared to sham stimulation (**Fig. 3e**). In contrast, when LC inhibition started once the permissive (Perm) period arrived, repeated REMS entries took place from the onset of the illumination at a frequency that markedly increased compared to Sham stimulation (**Fig. 3f**). In the latter case, the increased time spent in REMS came at the expense of NREMS time. In the former, times spent in both wake and NREMS were changed, suggesting that LC activity at the onset played additional roles for the subsequent NREMS bout architecture. Histological analysis supported the appropriate location of the optic fiber (**Suppl. Fig. 3b**). The functional efficiency of the optogenetic inhibition of LC was supported by a linear correlation between the light-induced changes in sleep spindle density and the increase in REMS transitions during Perm (**Suppl. Fig. 3c**). LC activity fluctuations seemed thus relevant for the time evolution of a normal NREM-REMS cycle, in part because they may have prevented precocious REMS entries during NREMS.

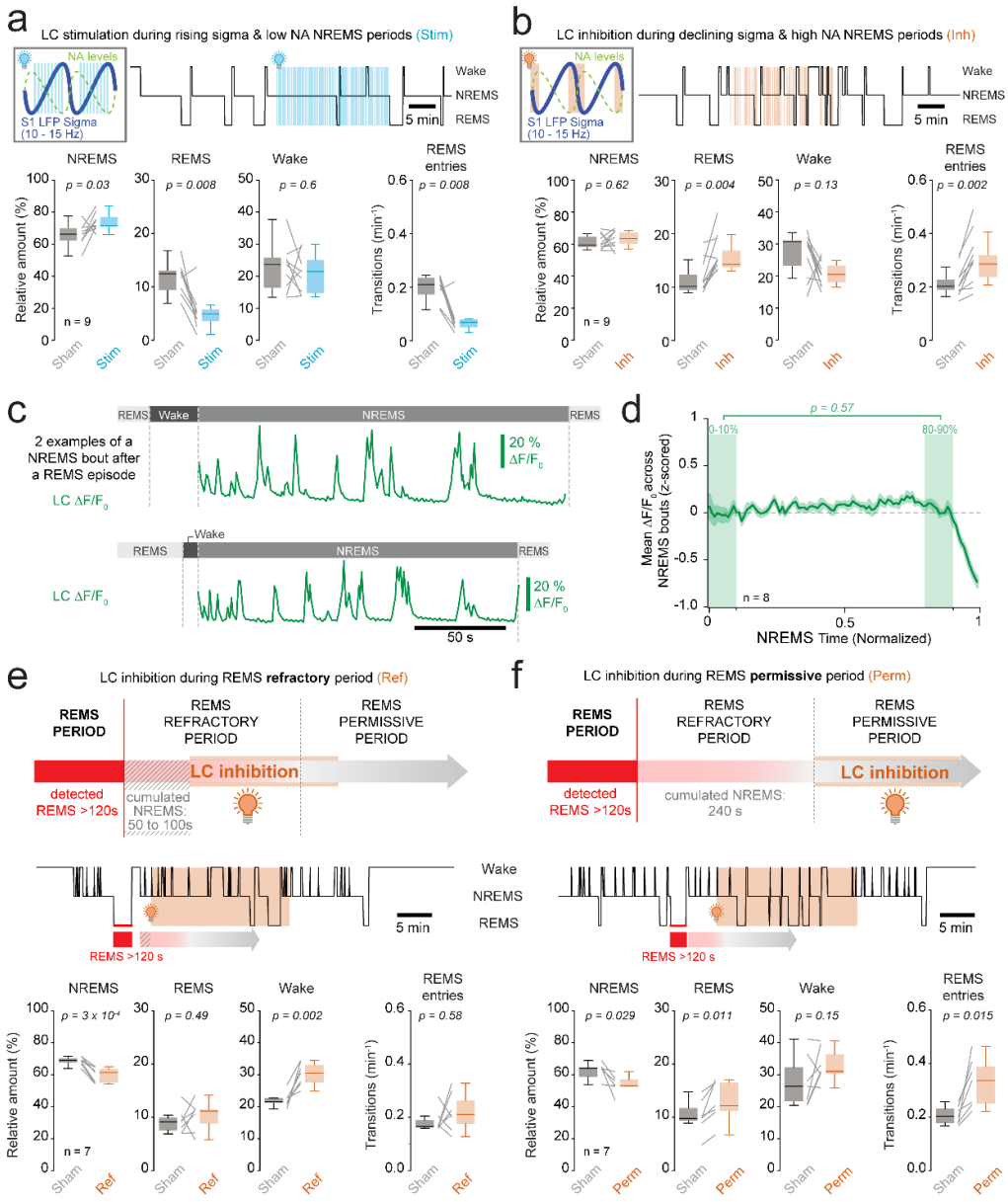

Figure 3. LC activity declines were necessary and sufficient for REMS entries in the natural NREMS-REMS cycle, except for a post-REMS refractory period.

a) Optogenetic stimulation of LC. Top, Schematic of the light stimulation protocol based on closed-loop feedback analysis of σ power, with corresponding NA levels indicated with green dotted line. Blue vertical lines show timing of optogenetic stimulation. Example histogram with stimulation periods indicated on the right. Box-and-whisker-plot quantifications of mean percentage times spent in Wake, NREMS and REMS and frequency of REMS entries, calculated for the 20-min light *vs* sham stimulation periods. Grey lines show paired datasets per animal. Wilcoxon signed-rank tests.

b) As a), for optogenetic inhibition of LC.

c) Example traces for LC fluorescence during NREMS bouts preceded and followed by REMS.

d) Mean LC fluorescence activity across NREMS bouts normalized in time. Shaded areas show data used for statistical analysis. Paired t-test.

e) Top, schematic of the LC inhibition protocol starting during the putative REMS refractory period (Ref), with temporal parameters taken from[39]. Example hypnogram is presented below. Quantification as described in a). Wilcoxon signed-rank or paired t-test.

f) As e, for LC inhibition starting after in the REMS-permissive period (Perm) that follows Ref. Wilcoxon signed-rank or paired t-tests.

See Supplementary Table 1 for detailed statistical information.

REMS entries occurred no faster than on infraslow time intervals during REMS restriction

As LC activity fluctuations needed to decay from high to low levels for a REMS entry, we thought that this should generate a minimum, non-reducible duration of NREMS that must complete before REMS could start. To test this, we aimed to increase specifically the frequency of REMS entries to study their timing relative to LC activity declines. We hence developed a REMS restriction (REMS-R) method in mice designed to maximally reduce time spent in REMS while preserving NREMS time. We used vibrating motors from cell phones that we taped to the animals' headstage to interrupt REMS in closed loop feedback (**Fig. 4a**)[15]. Starting at ZT0, these motors vibrated after 2 s of automatically detected REMS. Vibrations induced a brief arousal after which animals returned to NREMS. When interrupting every detected entry into REMS over a 6-h period from ZT0-ZT6, we observed a strong increase in attempts to enter REMS (**Fig. 4b**). No such increase was observed in the baseline recordings or in the yoked control animals that were exposed to vibration signals based on REMS detection from an animal in a neighboring cage. Both REMS-restricted and yoked controls showed comparable and relatively small losses in times spent in NREMS whereas more time was spent in wakefulness (**Suppl. Fig. 4a**). We ensured that this reduction of NREMS did not change NREMS pressure by verifying that the homeostatic decline in δ (1 – 4 Hz) power across the 12 h-light phase was comparable between groups (**Suppl. Fig. 4b**). Furthermore, REMS-restricted but not yoked controls showed a rebound in REMS time after REMS-R (**Suppl. Fig. 4c**).

We examined the timing of REMS entries with respect to fiber photometric measures of LC activity during REMS-R in a separate group of 6 animals. The mean duration of REMS bouts during the REMS-R was 6.1 ± 0.3 s (n = 6), and it was followed by an awakening lasting on average 29.7 ± 4.0 s (n = 6), similar to the recently reported values of another automated REMS-R method[40]. Aligning LC activity to REMS entries revealed that every REMS onset remained invariably preceded by a decline of LC activity (**Fig. 4c**). Furthermore, although REMS-R shortened the time between consecutive REMS entries, these remained locked to moments of low LC activity levels (**Fig. 4d**), with the mean interval between two entries settling at 40.5 ± 5.1 s at ZT6 (**Fig. 4e1**). When calculating LC activity levels in the

last 5 s before every REMS entry across the full time of REMS-R, we found these levels to remain constant during the entire REMS-R (**Fig. 4e2**). A decline of LC activity thus remained obligatory for a REMS entry, even when homeostatic REMS pressure was high. Accordingly, the decline of LC activity fluctuations generated a non-reducible time interval over which NREMS proceeded before a REMS entry took place.

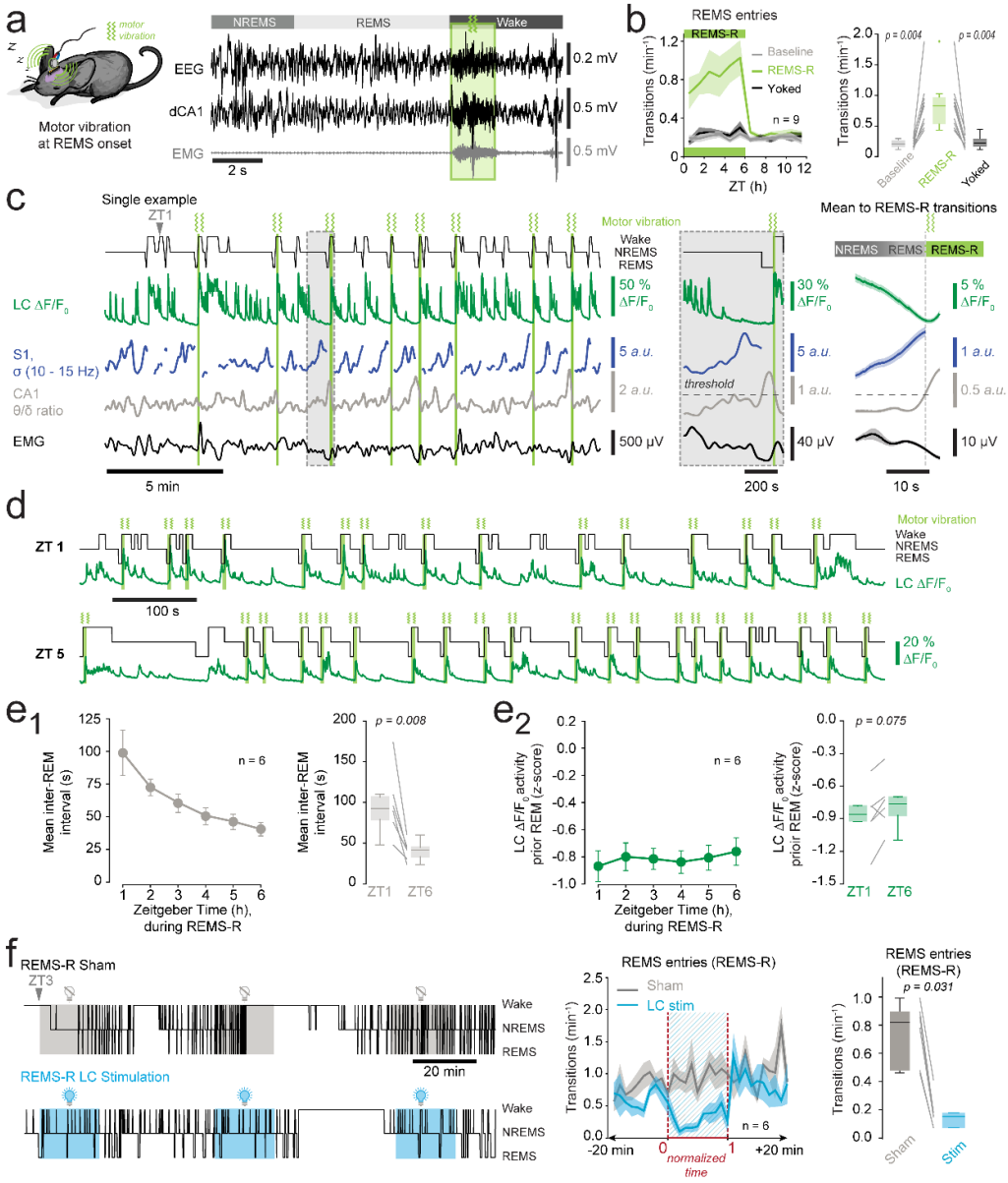

Figure 4. A REMS restriction (REMS-R) unraveled a non-reducible time interval between successive REMS entries.

a) Schematic of REMS-R implementation and representative recording showing effects of a single 2-s motor vibration after REMS onset (green rectangle with motor vibration symbol).

b) Frequency of REMS entries in animals subjected to REMS-R from ZT0-ZT6, for yoked animals (that received vibrations timed to REMS from their neighboring animal) and undisturbed controls. Box-and-whisker plot quantifications of mean data, with grey lines showing paired data for individual animals. Wilcoxon signed-rank test.

c) Example recording during a REMS-R, with expanded portion on the right (grey rectangle). Mean transitional dynamics calculated as in Fig. 2c (without addition of individual sleep spindles).

d) Example recording from a REMS-R at ZT1 and later at ZT5.

e) e1) Quantification of mean (inter-REM) intervals shown in d across the 6 h of REMS-R, with values for ZT1 and ZT6 shown in box-and-whisker plots on the right; e2) Same for LC activity levels in the 5 s before REMS entries. Grey lines connect paired data per animal. Paired t-tests for e1 and e2.

f) Example recording for a REMS-R combined with Sham or optogenetic stimulation of LC at 1 Hz. Quantification of REMS entries across the stimulation period. Note the higher REMS transition frequency before optogenetic stimulation compared to baseline sleep (Fig. 3a, b). Box-and-whisker quantification of mean data for the entire REMS-R. Wilcoxon signed-rank test.

See Supplementary Table 1 for detailed statistical information.

We finally verified whether LC activity was sufficient to suppress REMS entries even when the pressure to do so was elevated. We hence combined optogenetic LC stimulation in ChR2-expressing DBH-Cre animals with REMS-R (**Fig. 4f**). LC was stimulated at 1 Hz for 20 min per h, as done in baseline conditions (see Fig. 3). At all moments during REMS-R, LC stimulation rapidly and strongly suppressed REMS entries for the duration of the stimulation in a reversible manner, whereas sham stimulation showed no effect. This indicates that moderate levels of LC activity (1 Hz) override effects of REMS pressure on REMS entries.

A stimulus-enriched wake experience increased LC activity and disrupted subsequent sleep

Are LC activity fluctuations during NREMS dependent on how LC became engaged in a preceding wakefulness? We subjected jGCaMP8s-expressing DBH-Cre mice to two different 4 h-long sleep deprivation (SD) procedures from ZT0-ZT4 (**Fig. 5a**). One SD was achieved by the 'gentle handling' technique that softly interferes with the animals' spontaneous sleep-wake behavior to prevent sleep, minimally exposing the animals to potentially surprising stimuli that could activate LC. The stimulus-enriched SD (SSD) was enriched in auditory and somatosensory stimulation, to which the animals were not previously habituated and exposed to at irregular times, thus plausibly promoting LC activation (see Methods). Both SD and the SSD were carried out at least 2 weeks apart in groups of 4 animals. Blood sampling immediately after the SSD in a separate group of animals revealed increases in corticosterone levels compared to baseline (50.2 ± 11.9 ng /ml vs 314.5 ± 12.5 ng/ml, n = 8, $p = 4*10^{-6}$), indicating elevation of stress levels in addition to the sensory exposure, which strongly implicates

LC[41]. Conversely, we previously showed that gentle SD instead does not increase corticosterone levels[42].

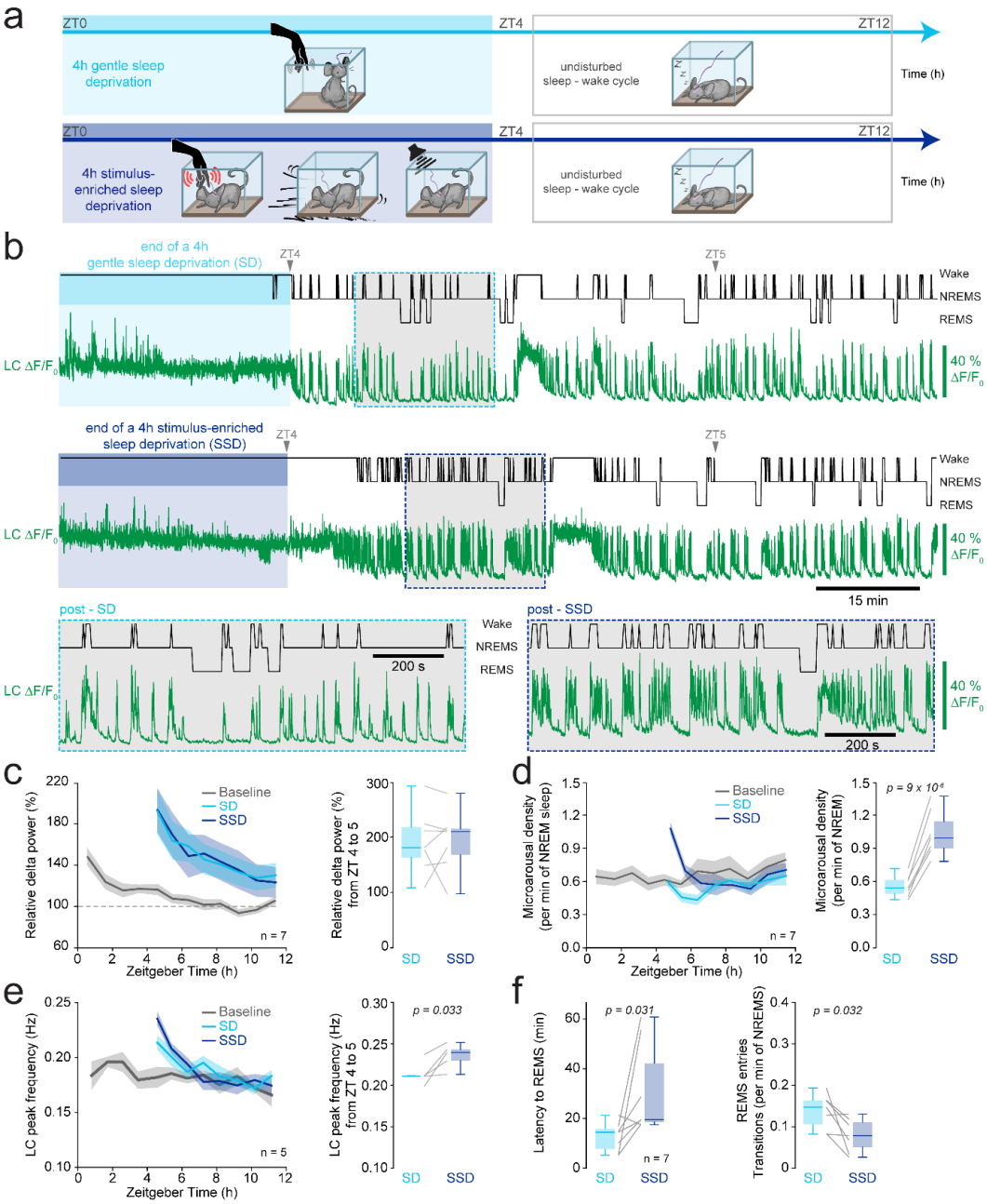

Figure 5. A stimulus-enriched but not a gentle sleep deprivation disrupted subsequent sleep and enhanced LC activity

a) Schematic of gentle sleep deprivation (SD) and stimulus-enriched sleep deprivation (SSD) procedures. For details of the stimuli used for SSD, see Methods.

b) Example hypnograms and corresponding LC fluorescence in sleep-wake behaviors following a 4-h SD or a 4-h SSD. Dotted rectangles indicate expanded portions below.

c) Mean dynamics of EEG δ power from ZT0-ZT12 for 7 animals subjected to baseline recordings, SD and SSD. Box-and-whisker quantification on the right, with grey lines showing paired data per animal. Paired t-test.

d) As c, for the density of MAs. Paired t-test.

e) As c, for LC peak frequency. Paired t-test.

f) Box-and-whisker quantification for REMS onset latency, quantified from the time of NREMS onset, and the frequency of REMS entries, for the first h after SD or SSD (ZT4-ZT5). Paired t-tests.

See Supplementary Table 1 for detailed statistical information.

Figure 5b shows two representative recordings of sleep-wake behavior immediately after SD or SSD of the same animal, illustrating that both LC activity and sleep architecture were differentially affected. Remarkably, both SD and SSD resulted in comparable increases in power of the EEG δ (1.5 – 4 Hz) band, indicating that the sleep pressure had become elevated similarly for both types of wake experiences (**Fig. 5c**). In contrast, the density of MAs changed in opposite directions for SSD compared to SD. SD decreased MA frequency in subsequent NREMS, which supports sleep consolidation as a result of SD[43]. The SSD instead resulted in a marked increase in MA density and hence fragmented NREMS (**Fig. 5d**). Furthermore, LC activity, measured in peak frequency, was higher in the first hour of SSD compared to SD (**Fig. 5e**). Finally, the latency to REMS onset was increased in SSD compared to SD and the number of transitions decreased within ZT4-ZT5 (**Fig. 5f**). A stimulus-enriched wake experience combined with stress thus transiently increased LC activity and disrupted sleep architecture for a transient post-SD/-SSD period of 1-2 h.

Increased LC activity underlay sleep disruptions after a stimulus-enriched wake experience

We examined LC's role for the SSD-induced sleep disruptions. First, we verified how LC fluctuations were associated with arousability and REMS entries. LC activity transients remained associated with spectral changes in the EEG that were similar to baseline conditions, but increases in δ (1.5 – 4 Hz) power for non-MA associated events were weakened (**Fig. 6a**). All REMS entries also remained invariably associated with LC activity declines (**Fig. 6b**). Second, to causally test the consequences of elevated LC activity, we subjected 8 Jaws-expressing DBH-Cre animals to two SSDs spaced at least 2 weeks apart, of which one was followed by 1 or 2 h of Jaws-mediated partial bilateral inhibition of LC, the other one by sham light exposure, in a counterbalanced manner. LC inhibition reduced the fragmentation of NREMS by microarousals in all 8 mice (**Fig. 6c**). Furthermore, REMS onset latency was shortened. The type of wake experience thus modified LC's activity fluctuations in NREMS to increase arousability and delaying REMS. Together, these are hallmarks of a deteriorated quality of sleep, to which abnormal LC activity contirbuted.

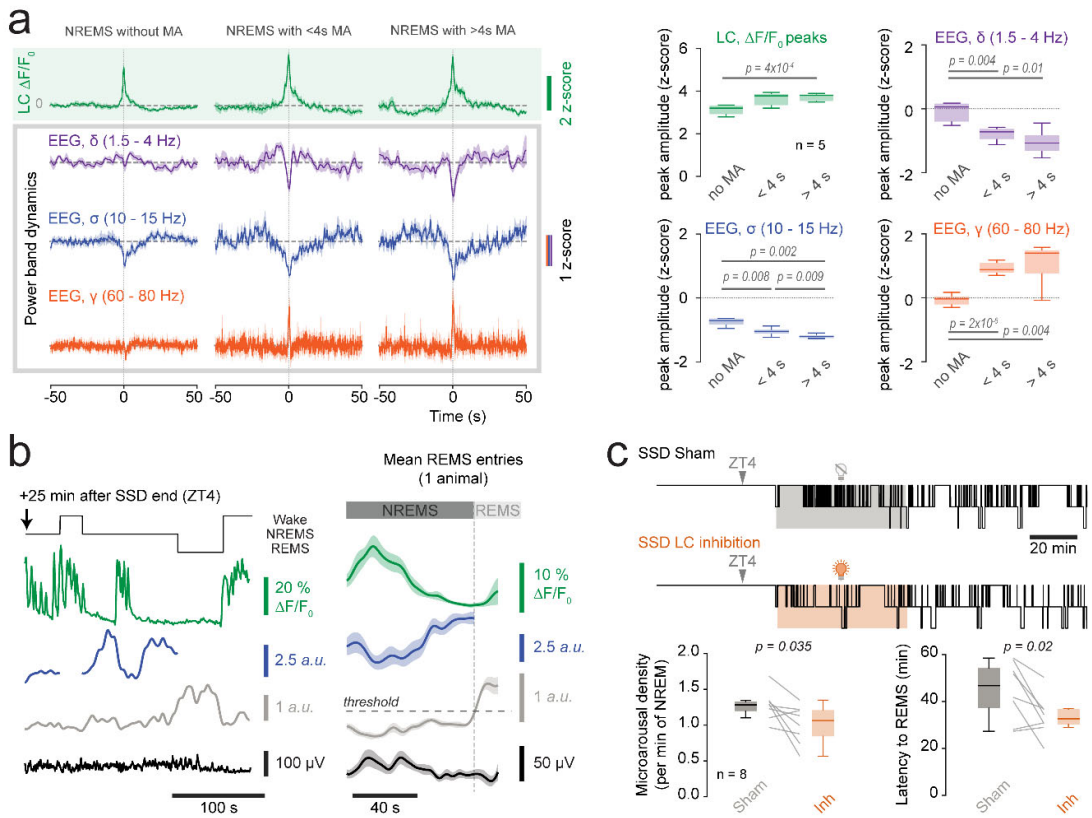

Figure 6. Acute LC inhibition suppressed sleep-disruptive effects of a stimulus-enriched wakefulness

a) Spectral analysis of EEG signals corresponding to LC fluorescence transients that are classified based on whether they did not or did co-occur with short (< 4 s) or long (> 4 s) microarousals for 2 h after SSD (ZT4-ZT6). Corresponding power dynamics for the δ, σ and γ frequency bands are aligned vertically (grey-lined box). Quantification of mean LC fluorescence and spectral transients between 0 – 5 s is shown on the right. One-way repeated-measures ANOVA followed by *post hoc* paired t-tests, with Bonferroni correction.

b) Example recording of a REMS entry after SSD. Mean transitional dynamics calculated as in Fig. 2c.

c) Example hypnogram after SSD with or without Jaws inhibition of LC.
Box-and-whisker quantification of MA density and REMS onset latency after SSD with sham or light stimulation. Paired t-test.

See Supplementary Table 1 for detailed statistical information.

Discussion

We identify the noradrenergic LC as a gatekeeper for the partitioning of mammalian sleep into NREMS and REMS. We probed LC's role for sleep by obtaining population measures of its activity in undisturbed sleep and during REMS restriction. We then interfered with this activity using optogenetic techniques in closed-loop feedback and analyzed consequences on sleep architecture. We found that,

on the one hand, the LC activity fluctuations were indispensable for the natural progression of undisturbed sleep. Most importantly, LC fluctuations set the windows of opportunity for transitions from NREMS to REMS, segregating them strictly from moments of high arousability. On the other hand, while being vital for natural sleep, LC activity in NREMS constituted a risk for acute sleep disruptions because of a high susceptibility to the preceding wake experience. The results presented in this study thus offer insight into the neural foundations of sleep's organization into NREMS-REMS cycles and they advance the mechanistic understanding of acute sleep disruptions.

To date, we know much about the neural circuits underlying NREMS and REMS individually. It is also well-established that both NREMS and REMS play important roles in sleep's restorative and memory-promoting functions[44-46]. The mechanisms underlying the alternation between NREMS and REMS have instead remained less clear, in spite of much phenomenological evidence that times spent in NREMS and REMS are interdependent[39,47-50], and that NREMS and REMS may be functionally complementary[51-57 58]. Furthermore, comparative studies showing ancestral forms of sleep in non-mammalian vertebrates indicate that alternations between states are evolutionarily preserved[55,57]. Recent studies have provided initial evidence for the neural control of the alternation between NREMS and REMS during the NREMS-REMS cycle[37,38,59]. The addition of the LC as a gatekeeper in this alternation is conceptually novel because it imposes a time constraint that gates the operation of these circuits.

The LC has been repeatedly linked to the suppression of REMS[7], yet here we probed this link in the natural NREMS-REMS cycle through optogenetic interference according to statistical models of the mouse NREMS-REMS cycle[39]. We found LC activity to be relevant for preventing precocious REMS entries throughout much of this cycle. This suggests that REMS entries can be attempted early in a NREMS bout, even when homeostatic effects are comparatively low. In support of this possibility, the inhibitory paragigantocellular reticular nucleus shows infraslow fluctuations during much of NREMS and can inhibit LC, thus possibly leading to an on-going drive for REMS[34,38]. We also tested here for the first time the REMS refractory period in a closed-loop setting[60]. Inhibiting LC starting from the onset of this period was not sufficient to recover REMS entries. However, the data support the existence of an early post-REMS phase during which LC activity shapes the architecture of the ensuing NREMS bout. Further refinement of the optogenetic inhibition protocols are necessary to understand the basis of the refractory period and how it connects with the gatekeeping role of LC in the subsequent permissive period.

We found no evidence for a NREMS-dependent homeostatic regulation of LC activity, although we cannot exclude such regulation for LC neuronal subgroups in specific REMS-regulatory networks.

In comparison, REMS-inhibiting ventrolateral periaqueductal gray neurons show a gradual decline in activity during NREMS bouts. They could hence be relevant for the homeostatic increase in REMS pressure by NREMS duration[37]. Furthermore, REMS-promoting and LC-inhibiting dorsal paragigantocellular reticular neurons show augmenting activity with time spent in NREMS, reaching a maximum just prior to REMS[34,38]. Cholinergic neurons in the mesopontine tegmentum strongly increase discharge just before a REMS entry[61-63] and optogenetic stimulation increases the frequency of REMS entries[64]. In comparison, LC fluctuated stably during NREMS and could hence coordinate the unfolding of REMS-promoting conditions at appropriate time points. Of particular interest is the observation that these conditions are segregated from moments of elevated arousability. This suggests that LC's gatekeeping role ensures REMS cannot take place unless the brain is optimally protected from external interference. Further possible roles of LC for REMS, including its maintenance and termination, but also its maladaptive roles, remain to be investigated.

The gatekeeping role of LC was strikingly evident when REMS entries became very frequent during REMS-R. The specificity of the REMS-R procedure, which minimally affected time spent in NREMS and wakefulness, was essential for this purpose because it allowed to preserve LC activity from confounding effects of altered sleep-wake architecture. Our method is thus an important contribution to automated approaches for REMS restriction[40]. Although the motor-induced awakenings elevated LC activity transiently, there was enough NREMS present in between attempts to demonstrate the continued necessity of LC troughs for the NREMS-to-REMS transitions, which resulted in a non-reducible time interval of 30 – 50 s in between attempts. Intriguingly, such a minimal time interval has been previously observed in REMS-restriction protocols of similar duration, which involved electrical stimulation of the serotoninergic dorsal raphe[65] or manual stimulation of the animal[66]. Insight into the dynamics of LC activity provides an explanation for this observation.

Surprisingly, LC activity transients increased δ (1.5 – 4 Hz) power in both the local LFP and the global EEG recordings. This was not expected based on the widely documented desynchronizing actions of LC stimulation on the EEG[3]. The finding is a clear sign that the relationship between LC activity levels, the discharge pattern of individual units (e.g. burst vs tonic)[10], and the effects on the state of the forebrain need to be further dissected to appreciate the full diversity of LC operations. It is also possible that LC neuronal populations act in heterogeneous subgroups with different activity profiles and output connectivities[1,67]. Advancing in such functional dissection of LC neurons will be critical in balancing debates on whether LC is primarily sleep-promoting or sleep-disruptive[27]. Our data start to resolve this by offering a systematic analysis of the spectral profile of LC activity transients. The LC-induced increase in δ (1.5 – 4 Hz) power indicates that low-frequency activity patterns traditionally

associated with deeper NREMS are instead a forebrain manifestation of activated brainstem arousal circuits.

EEG hallmarks indicating that NREMS consolidation is strengthened (through δ power increases) while arousability is high has been similarly described for a large spike-like EEG signal in the human NREMS EEG, referred to as 'K-complex'[68]. The K-complex preferentially appears in the 'light' sleep stage N2, either spontaneously or in response to sensory stimuli. K-complexes can occur in infraslow sequences and show intracranial spectral profiles similar to what we describe here[69,70]. In the early phase of falling asleep, some K-complexes have been linked to a 'bottom-up', arousal system-dependent process[70]. Although more work is needed to establish the spatiotemporal and functional profile of LC-induced δ activity, our findings could help in the functional classification of sleep slow waves and in the search for possible EEG read-outs of LC activity in human sleep.

The noradrenergic LC is implied in neuronal, glial and vascular control processes in the brain[7], raising the possibility that some of these could be relevant to understand LC's gatekeeping role. The LC activity fluctuations generate a clustering of sleep spindles over 30 – 50 s[11], which are important for sleep-dependent memory consolidation[14,44], probably through regulation of cortical dendritic excitability[71] and excitation-inhibition balance[58]. It is intriguing to note that a minimal NREMS bout length of at least 60 s was required for declarative memory consolidation in rodent[72]. Through its terminal innervation of components of the neurovascular unit[73], a structural assembly of neural, vascular and endothelial elements, LC activity may contribute to interplay between neural activity, blood flow, and cerebrospinal fluid exchange. Here, infraslow time scales are considered particularly effective for the arterial vasomotion underlying the coupling between blood volume and cerebrospinal fluid influx[74]. The LC could coordinate diverse beneficial consequences of NREMS on an infraslow time scale, aligning its neuroprotective and plasticity-promoting functions in time. Clearly, more work is needed to determine what causes the LC to show infraslow activity transients to get insights into this possibility.

An aversive or stressful experience in humans can be followed by an acute insomnia characterized by increased sleep fragmentation and alterations in REMS properties[75,76]. Several recent studies have identified the LC to be involved in sleep disruptions preceded by acute stressful experiences[17,77], illustrating the growing recognition for neural circuits involving monoamine release as source for sleep disturbances. As LC controls both, spontaneous arousability and REMS gating, alterations in its activity could be particularly risky for sleep. Furthermore, the degree by which LC activity is altered seemed to depend on the type of wake experience. In a rodent study on the highly stressful social defeat paradigms, LC activity fluctuations in NREMS were replaced by irregular

activity[17]. In comparison, SSD preserved the fluctuating pattern in our experiments. The degree of LC activity disruptions in NREMS could grade with the severity of the wake experience and cause different levels of sleep deterioration. Indeed, we found that REMS disruptions could be induced by low-frequency stimulation of LC at 1 Hz, which did not cause more MAs.

The study offers a neural mechanism relevant for the alternation of mammalian sleep between states of NREMS and REMS. We revise the notion for a general arousal-promoting of LC by identifying specific LC-dependent signatures of NREMS promotion that show a unique spectral profile so far not described in rodent sleep. LC activity preserved the windows of opportunity for REMS entries even when the pressure for REMS was high, thus strictly gatekeeping the time of NREMS before REMS. Elucidating the origins of this temporal constraint could shine light on some of the NREMS functions that must invariably be coordinated or take some time to be completed so that REMS can take over. The susceptibility of sleep-active LC to the preceding wake experience further brings novel opportunities to elucidate sleep disruptions that could be impacted by the diversity of our daily experiences.

References

1 Poe, G. R. *et al.* Locus coeruleus: a new look at the blue spot. *Nat Rev Neurosci* **21**, 644-659, doi:10.1038/s41583-020-0360-9 (2020).

2 Aston-Jones, G. & Cohen, J. D. An integrative theory of locus coeruleus-norepinephrine function: adaptive gain and optimal performance. *Annu Rev Neurosci* **28**, 403-450, doi:10.1146/annurev.neuro.28.061604.135709 (2005).

3 Berridge, C. W. Noradrenergic modulation of arousal. *Brain Res Rev* **58**, 1-17, doi:10.1016/j.brainresrev.2007.10.013 (2008).

4 Rajkowski, J., Kubiak, P. & Aston-Jones, G. Locus coeruleus activity in monkey: phasic and tonic changes are associated with altered vigilance. *Brain Res Bull* **35**, 607-616, doi:10.1016/0361-9230(94)90175-9 (1994).

5 Reimer, J. *et al.* Pupil fluctuations track rapid changes in adrenergic and cholinergic activity in cortex. *Nat Commun* **7**, 13289, doi:10.1038/ncomms13289 (2016).

6 Saper, C. B., Fuller, P. M., Pedersen, N. P., Lu, J. & Scammell, T. E. Sleep state switching. *Neuron* **68**, 1023-1042, doi:10.1016/j.neuron.2010.11.032 (2010).

7 Osorio-Forero, A., Cherrad, N., Banterle, L., Fernandez, L. M. J. & Lüthi, A. When the locus coeruleus speaks up in sleep: recent insights, emerging perspectives. *Int J Mol Sci* **23**, doi:10.3390/ijms23095028 (2022).

8 Morris, L. S., McCall, J. G., Charney, D. S. & Murrough, J. W. The role of the locus coeruleus in the generation of pathological anxiety. *Brain Neurosci Adv* **4**, 2398212820930321, doi:10.1177/2398212820930321 (2020).

9 Yu, X., Franks, N. P. & Wisden, W. Sleep and sedative states induced by targeting the histamine and noradrenergic Systems. *Front Neural Circuits* **12**, 4, doi:10.3389/fncir.2018.00004 (2018).

10 Eschenko, O., Magri, C., Panzeri, S. & Sara, S. J. Noradrenergic neurons of the locus coeruleus are phase locked to cortical up-down states during sleep. *Cereb Cortex* **22**, 426-435, doi:10.1093/cercor/bhr121 (2012).

11 Osorio-Forero, A. *et al.* Noradrenergic circuit control of non-REM sleep substates. *Curr Biol* **31**, 5009-5023 e5007, doi:10.1016/j.cub.2021.09.041 (2021).

12 Kjaerby, C. *et al.* Memory-enhancing properties of sleep depend on the oscillatory amplitude of norepinephrine. *Nat Neurosci* **25**, 1059-1070, doi:10.1038/s41593-022-01102-9 (2022).

13 Hayat, H. *et al.* Locus coeruleus norepinephrine activity mediates sensory-evoked awakenings from sleep. *Sci Adv* **6**, eaaz4232, doi:10.1126/sciadv.aaz4232 (2020).

14 Fernandez, L. M. J. & Lüthi, A. Sleep spindles: mechanisms and functions. *Physiol Rev* **100**, 805-868, doi:10.1152/physrev.00042.2018 (2020).

15 Cardis, R. *et al.* Local cortical arousals and heightened (somato)sensory arousability during non-REM sleep of mice in chronic pain. *Elife* **10**, e65835, doi:10.7554/eLife.65835 (2021).

16 Lecci, S. *et al.* Coordinated infra-slow neural and cardiac oscillations mark fragility and offline periods in mammalian sleep. *Sci. Adv.* **3**, e1602026, doi:10.1126/sciadv.1602026 (2017).

17 Antila, H. *et al.* A noradrenergic-hypothalamic neural substrate for stress-induced sleep disturbances. *Proc Natl Acad Sci U S A* **119**, e2123528119, doi:10.1073/pnas.2123528119 (2022).

18 Spiegel, R. & DeVos, J. E. Central effects of guanfacine and clonidine during wakefulness and sleep in healthy subjects. *Br J Clin Pharmacol* **10 Suppl 1**, 165S-168S, doi:10.1111/j.1365-2125.1980.tb04925.x (1980).

19 Nicholson, A. N. & Pascoe, P. A. Presynaptic alpha$_2$-adrenoceptor function and sleep in man: studies with clonidine and idazoxan. *Neuropharm* **30**, 367-372, doi:10.1016/0028-3908(91)90062-g (1991).

20 Palagini, L., Baglioni, C., Ciapparelli, A., Gemignani, A. & Riemann, D. REM sleep dysregulation in depression: state of the art. *Sleep Med Rev* **17**, 377-390, doi:10.1016/j.smrv.2012.11.001 (2013).

21 Koshmanova, E. *et al.* In vivo Locus Coeruleus activity while awake is associated with REM sleep quality in healthy older individuals. *bioRxiv*, doi:10.1101/2023.02.10.527974 (2023).

22 Zhang, Y. *et al.* Fast and sensitive GCaMP calcium indicators for imaging neural populations. *Nature*, doi:10.1038/s41586-023-05828-9 (2023).

23 Feng, J. *et al.* A genetically encoded fluorescent sensor for rapid and specific *in vivo* detection of norepinephrine. *Neuron* **102**, 745-761 e748, doi:10.1016/j.neuron.2019.02.037 (2019).

24 Foote, S. L., Aston-Jones, G. & Bloom, F. E. Impulse activity of locus coeruleus neurons in awake rats and monkeys is a function of sensory stimulation and arousal. *Proc Natl Acad Sci U S A* **77**, 3033-3037, doi:10.1073/pnas.77.5.3033 (1980).

25 Aston-Jones, G. & Bloom, F. E. Activity of norepinephrine-containing locus coeruleus neurons in behaving rats anticipates fluctuations in the sleep-waking cycle. *J Neurosci* **1**, 876-886, doi:10.1523/JNEUROSCI.01-08-00876.1981 (1981).

26 Tobler, I., Deboer, T. & Fischer, M. Sleep and sleep regulation in normal and prion protein-deficient mice. *J Neurosci* **17**, 1869-1879 (1997).

27 Lüthi, A., Franken, P., Fulda, S., Siclari, F., Van Someren E.J.W. Do all noradrenaline surges disrupt sleep? *Nat Neurosci*, in press, doi:10.1038/s41593-023-01313-8 (2023).

28 Lee, K. H. & McCormick, D. A. Abolition of spindle oscillations by serotonin and norepinephrine in the ferret lateral geniculate and perigeniculate nuclei *in vitro*. *Neuron* **17**, 309-321, doi:10.1016/s0896-6273(00)80162-2 (1996).

29 Fernandez, L. M. *et al.* Thalamic reticular control of local sleep in sensory cortex. *Elife* **7**, e39111, doi:10.7554/eLife.39111 (2018).

30 Gottesmann, C. The transition from slow-wave sleep to paradoxical sleep: evolving facts and concepts of the neurophysiological processes underlying the intermediate stage of sleep. *Neurosci Biobehav Rev* **20**, 367-387 (1996).

31 Sullivan, D., Mizuseki, K., Sorgi, A. & Buzsáki, G. Comparison of sleep spindles and theta oscillations in the hippocampus. *J Neurosci* **34**, 662-674, doi:10.1523/JNEUROSCI.0552-13.2014 (2014).

32 Durán, E., Oyanedel, C. N., Niethard, N., Inostroza, M. & Born, J. Sleep stage dynamics in neocortex and hippocampus. *Sleep* **41**, zsy060, doi:10.1093/sleep/zsy060 (2018).

33 Kaur, S., Saxena, R. N. & Mallick, B. N. GABAergic neurons in prepositus hypoglossi regulate REM sleep by its action on locus coeruleus in freely moving rats. *Synapse* **42**, 141-150, doi:10.1002/syn.1109 (2001).

34 Goutagny, R. *et al.* Role of the dorsal paragigantocellular reticular nucleus in paradoxical (rapid eye movement) sleep generation: a combined electrophysiological and anatomical study in the rat. *Neuroscience* **152**, 849-857, doi:10.1016/j.neuroscience.2007.12.014 (2008).

35 Franken, P. Long-term vs. short-term processes regulating REM sleep. *J Sleep Res* **11**, 17-28 (2002).

36 Luppi, P. H. *et al.* Paradoxical (REM) sleep genesis: the switch from an aminergic-cholinergic to a GABAergic-glutamatergic hypothesis. *J Physiol Paris* **100**, 271-283, doi:10.1016/j.jphysparis.2007.05.006 (2006).

37 Weber, F. *et al.* Regulation of REM and non-REM sleep by periaqueductal GABAergic neurons. *Nat Commun* **9**, 354, doi:10.1038/s41467-017-02765-w (2018).

38 Stucynski, J. A., Schott, A. L., Baik, J., Chung, S. & Weber, F. Regulation of REM sleep by inhibitory neurons in the dorsomedial medulla. *Curr Biol* **32**, 37-50 e36, doi:10.1016/j.cub.2021.10.030 (2022).

39 Park, S. H. *et al.* A probabilistic model for the ultradian timing of REM sleep in mice. *PLoS Comput Biol* **17**, e1009316, doi:10.1371/journal.pcbi.1009316 (2021).

40 Arthaud, S., Libourel, P. A., Luppi, P. H. & Peyron, C. Insights into paradoxical (REM) sleep homeostatic regulation in mice using an innovative automated sleep deprivation method. *Sleep* **43**, doi:10.1093/sleep/zsaa003 (2020).

41 Floriou-Servou, A. *et al.* The acute stress response in the multiomic era. *Biol Psychiatry* **89**, 1116-1126, doi:10.1016/j.biopsych.2020.12.031 (2021).

42 Kopp, C., Longordo, F., Nicholson, J. R. & Lüthi, A. Insufficient sleep reversibly alters bidirectional synaptic plasticity and NMDA receptor function. *J Neurosci* **26**, 12456-12465, doi:10.1523/JNEUROSCI.2702-06.2006 (2006).

43 Franken, P., Malafosse, A. & Tafti, M. Genetic determinants of sleep regulation in inbred mice. *Sleep* **22**, 155-169 (1999).

44 Brodt, S., Inostroza, M., Niethard, N. & Born, J. Sleep-A brain-state serving systems memory consolidation. *Neuron* **111**, 1050-1075, doi:10.1016/j.neuron.2023.03.005 (2023).

45 Morrison, M., Halson, S. L., Weakley, J. & Hawley, J. A. Sleep, circadian biology and skeletal muscle interactions: Implications for metabolic health. *Sleep Med Rev* **66**, 101700, doi:10.1016/j.smrv.2022.101700 (2022).

46 Oesch, L. T. & Adamantidis, A. R. How REM sleep shapes hypothalamic computations for feeding behavior. *Trends Neurosci* **44**, 990-1003, doi:10.1016/j.tins.2021.09.003 (2021).

47 Hartmann, E. Mechanism underlying the sleep-dream cycle. *Nature* **212**, 648-650, doi:10.1038/212648b0 (1966).

48 Benington, J. H. & Heller, H. C. REM-sleep timing is controlled homeostatically by accumulation of REM-sleep propensity in non-REM sleep. *Am J Physiol* **266**, R1992-2000, doi:10.1152/ajpregu.1994.266.6.R1992 (1994).

49 Vivaldi, E. A., Ocampo, A., Wyneken, U., Roncagliolo, M. & Zapata, A. M. Short-term homeostasis of active sleep and the architecture of sleep in the rat. *J Neurophysiol* **72**, 1745-1755, doi:10.1152/jn.1994.72.4.1745 (1994).

50 Benington, J. H. & Heller, H. C. Does the function of REM sleep concern non-REM sleep or waking? *Prog Neurobiol* **44**, 433-449, doi:10.1016/0301-0082(94)90005-1 (1994).

51 Ephron, H. S. & Carrington, P. Rapid eye movement sleep and cortical homeostasis. *Psychol Rev* **73**, 500-526, doi:10.1037/h0023888 (1966).

52 Wehr, T. A. A brain-warming function for REM sleep. *Neurosci Biobehav Rev* **16**, 379-397, doi:10.1016/s0149-7634(05)80208-8 (1992).

53 Vertes, R. P. A life-sustaining function for REM sleep: a theory. *Neurosci Biobehav Rev* **10**, 371-376, doi:10.1016/0149-7634(86)90002-3 (1986).

54 Kavanau, J. L. Evolutionary aspects of sleep and its REM and NREM states. *Adv Cell Aging and Gerontol* **17**, 1-32, doi:10.1016/S1566-3124(05)17001-1 (2005).

55 Yamazaki, R. *et al.* Evolutionary origin of distinct NREM and REM sleep. *Front Psychol* **11**, 567618, doi:10.3389/fpsyg.2020.567618 (2020).

56 Le Bon, O. Relationships between REM and NREM in the NREM-REM sleep cycle: a review on competing concepts. *Sleep Med* **70**, 6-16, doi:10.1016/j.sleep.2020.02.004 (2020).

57 Blumberg, M. S., Lesku, J. A., Libourel, P. A., Schmidt, M. H. & Rattenborg, N. C. What is REM sleep? *Curr Biol* **30**, R38-R49, doi:10.1016/j.cub.2019.11.045 (2020).

58 Niethard, N., Brodt, S. & Born, J. Cell-type-specific dynamics of calcium activity in cortical circuits over the course of slow-wave sleep and rapid eye movement sleep. *J Neurosci* **41**, 4212-4222, doi:10.1523/JNEUROSCI.1957-20.2021 (2021).

59 Hayashi, Y. *et al.* Cells of a common developmental origin regulate REM/non-REM sleep and wakefulness in mice. *Science* **350**, 957-961, doi:10.1126/science.aad1023 (2015).

60 Le Bon, O. An asymmetrical hypothesis for the NREM-REM Sleep alternation-what is the NREM-REM cycle? *Front Neurosci* **15**, 627193, doi:10.3389/fnins.2021.627193 (2021).

61 Boucetta, S., Cissé, Y., Mainville, L., Morales, M. & Jones, B. E. Discharge profiles across the sleep-waking cycle of identified cholinergic, GABAergic, and glutamatergic neurons in the pontomesencephalic tegmentum of the rat. *J Neurosci* **34**, 4708-4727, doi:10.1523/JNEUROSCI.2617-13.2014 (2014).

62 Kayama, Y., Ohta, M. & Jodo, E. Firing of 'possibly' cholinergic neurons in the rat laterodorsal tegmental nucleus during sleep and wakefulness. *Brain Res* **569**, 210-220 (1992).

63 el Mansari, M., Sakai, K. & Jouvet, M. Unitary characteristics of presumptive cholinergic tegmental neurons during the sleep-waking cycle in freely moving cats. *Exp Brain Res* **76**, 519-529, doi:10.1007/BF00248908. (1989).

64 Van Dort, C. J. *et al.* Optogenetic activation of cholinergic neurons in the PPT or LDT induces REM sleep. *Proc Natl Acad Sci U S A* **112**, 584-589, doi:10.1073/pnas.1423136112 (2015).

65 Benington, J. H., Woudenberg, M. C. & Heller, H. C. REM-sleep propensity accumulates during 2-h REM-sleep deprivation in the rest period in rats. *Neurosci Lett* **180**, 76-80, doi:10.1016/0304-3940(94)90917-2 (1994).

66 Endo, T., Schwierin, B., Borbely, A. A. & Tobler, I. Selective and total sleep deprivation: effect on the sleep EEG in the rat. *Psychiatry Res* **66**, 97-110, doi:10.1016/s0165-1781(96)03029-6 (1997).

67 Totah, N. K., Neves, R. M., Panzeri, S., Logothetis, N. K. & Eschenko, O. The locus coeruleus is a complex and differentiated neuromodulatory system. *Neuron* **99**, 1055-1068 e1056, doi:10.1016/j.neuron.2018.07.037 (2018).

68 Halász, P. The K-complex as a special reactive sleep slow wave - a theoretical update. *Sleep Med Rev* **29**, 34-40 (2016).

69 Latreille, V. *et al.* The human K-complex: Insights from combined scalp-intracranial EEG recordings. *Neuroimage* **213**, 116748, doi:10.1016/j.neuroimage.2020.116748 (2020).

70 Siclari, F. *et al.* Two distinct synchronization processes in the transition to sleep: a high-density electroencephalographic study. *Sleep* **37**, 1621-1637, doi:10.5665/sleep.4070 (2014).

71 Seibt, J. *et al.* Cortical dendritic activity correlates with spindle-rich oscillations during sleep in rodents. *Nat Commun* **8**, 684, doi: 10.1038/s41467-017-00735-w (2017).

72 Rolls, A. *et al.* Optogenetic disruption of sleep continuity impairs memory consolidation. *Proc Natl Acad Sci U S A* **108**, 13305-13310, doi:10.1073/pnas.1015633108 (2011).

73 Giorgi, F. S. *et al.* Locus Coeruleus and neurovascular unit: from its role in physiology to its potential role in Alzheimer's disease pathogenesis. *J Neurosci Res* **98**, 2406-2434, doi:10.1002/jnr.24718 (2020).

74 Lewis, L. D. The interconnected causes and consequences of sleep in the brain. *Science* **374**, 564-568, doi:10.1126/science.abi8375 (2021).

75 Deliens, G., Gilson, M. & Peigneux, P. Sleep and the processing of emotions. *Exp Brain Res* **232**, 1403-1414, doi:10.1007/s00221-014-3832-1 (2014).

76 Wassing, R. *et al.* Restless REM sleep impedes overnight amygdala adaptation. *Curr Biol* **29**, 2351-2358 e2354, doi:10.1016/j.cub.2019.06.034 (2019).

77 Lo, Y., Yi, P. L., Hsiao, Y. T. & Chang, F. C. Hypocretin in locus coeruleus and dorsal raphe nucleus mediates inescapable footshock stimulation (IFS)-induced REM sleep alteration. *Sleep* **45**, doi:10.1093/sleep/zsab301 (2022).

78 Owen, S. F. & Kreitzer, A. C. An open-source control system for in vivo fluorescence measurements from deep-brain structures. *J Neurosci Methods* **311**, 170-177, doi:10.1016/j.jneumeth.2018.10.022 (2019).

79 Sherathiya, V. N., Schaid, M. D., Seiler, J. L., Lopez, G. C. & Lerner, T. N. GuPPy, a Python toolbox for the analysis of fiber photometry data. *Sci Rep* **11**, 24212, doi:10.1038/s41598-021-03626-9 (2021).

80 Bettinardi, R. G. *distributionPlot_OnlyPositive*, 2023).

Materials and Methods

ANIMALS AND HUSBANDRY

The study used two mouse lines - the C57BL/6J line and the B6.FVB(Cg)-Tg(Dbh-cre)KH212Gsat/Mmucd (MMRRC Stock#036778-UCD) line, referred to here as DBH-Cre line, that was originally provided to us by David McCormick and Paul Steffan, University of Oregon. Mice were bred on a C57BL/6J background and housed in a humidity- and temperature-controlled animal house with a 12 h / 12 h light-dark cycle (lights on at 9 am, corresponding to ZT0). Food and water were available *ad libitum* throughout all experiments. For viral injections, 3- to 10-week-old mice of either sex were transferred to a housing cabinet in a P2 safety level room, where they stayed from 1 d before to 3 d after the viral injection. They were then transferred to the sleep-wake recording room and left to recover for ≥ 1 week before undergoing the implantation surgery, after which they were single-housed in standard-sized cages. The grids on top of the cage were removed and replaced by 30 cm-high Plexiglass walls. Fresh food was regularly placed on the litter and the water bottle inserted through a hole in the cage wall. Objects (tissues, paper rolls, ping-pong balls) were given for enrichment.

In total, 8 DBH-Cre mice were used for two 12-h baseline sleep recordings in the light phase in combination with fiber photometry under undisturbed conditions. One animal was excluded because the dynamic range of the fluorescent signal ($\Delta F/F_0 < 15\%$, see below). Additionally, two of these 2 DBH-Cre animals were used for combined fiber photometric monitoring of LC activity and NE levels, these were included in the analysis of LC fluorescence across wake, NREMS, REMS. For combined LC optogenetic inhibition with fiber photometric monitoring of NE release, 2 DBH-Cre animals were used. Of the 8 DBH-Cre animals included for fiber photometric monitoring of LC activity, six were used for 1-2 sessions of REMS-R in combination with fiber photometric monitoring of LC activity, and 7 of these mice additionally underwent 1-2 sessions of SD and one session of SSD, again in combination with fiber photometric monitoring of LC activity. Animals in which the dynamic range of fluorescence fell < 15% during repeated fiber photometric sessions were no longer included in the analysis of LC activity. 9

DBH-Cre mice for optogenetic stimulation and 9 DBH-Cre mice for optogenetic inhibition during different phases of the infraslow fluctuation in σ power were already used in an earlier study and re-analyzed here. Seven DBH-Cre mice were used for optogenetic inhibition in the REMS-refractory or –permissive period of the undisturbed NREMS-REMS cycle, and an additional 7 were used for control viral injections. For the validation of the REMS-R procedure alone, 9 C57BL/6J animals were used. For REMS-R in combination with optogenetic stimulation, 7 DBH-Cre animals were used. Eight animals were used for SSD in combination with optogenetic LC inhibition, and 2 for SSD with control virus injections. A separate group of 8 animals were used for quantification of corticosterone levels at ZT4 in baseline and after SSD. All experiments were conducted in accordance with the Swiss National Institutional Guidelines on Animal Experimentation and were approved by the Swiss Cantonal Veterinary Office Committee for Animal Experimentation.

VIRAL VECTORS AND INJECTIONS

General and local anesthesia, analgesia, temperature control, stereotaxic fixation and drilling of craniotomies for injections of viral vectors were as described [11]. For fiber photometric monitoring, DBH-Cre mice were unilaterally injected over the right LC (L 1.05; AP -5.4; DV -3.2) with AAV5.hSyn1.dlox.GCaMP8s.dlox.WPRE-SV40p(A) (300 nL, titer 5.8Ex10^{12} vg/ml, Viral Vector Facility (VVF) Zürich) at an injection rate of 50-100 nL/min using a thin glass pipette (5-000-1001-X, Drummond Scientific) pulled on a vertical puller (Narishige PP-830), initially filled with mineral oil, and backfilled with the virus-containing solution just prior to injection. For transfection of the LC for optogenetics, viral vectors injected were ssAAV5/2-hEF1α-dlox-hChR2(H134R)_mCherry(rev)-dlox-WPRE-hGHp(A) (9.1x10^{12} vg/ml, 0.8 – 1 µL, unilateral, VVF Zürich) or ssAAV-5/2-hSyn1-dlox-Jaws_KGC_EGFP_ERES(rev)-dlox-WPRE-bGHp(A)-SV40p(A) (6.4x10^{12} vg/ml, 300 nL bilateral, VVF Zürich). The control virus for Jaws experiments was ssAAV-5/2-EF1α-dlox-mCherry(rev)-dlox-WPRE-bGHp(A) (7.3x10^{12} vg/ml, 300 nL bilateral, VVF Zürich). For monitoring of free NA levels, ssAAV9/2-hSyn1-GRAB_NE1h-WPRE-hGHp(A) (7.2x10^{12} vg/ml; VVF Zürich) was injected unilaterally in primary somatosensory thalamus (500 nL; L 2.0; AP -1.6; D -3.0) as described before [11]. Two animals each were

dually injected for combined expression of jGCaMP8s and $GRAB_{NE1h}$ or Jaws and $GRAB_{NE1h}$ in the right hemisphere. After the injections, the incision was sutured and disinfected, and the animal was supervised and given paracetamol at 2 mg / ml for the next 4 days.

SURGERIES

Surgeries for sleep recordings. Surgeries for implantation of electrodes for sleep-wake monitoring were done at least 1 week after the viral injection. Following anesthesia induction (5% Isoflurane, animals were gas-anesthetized (Isoflurane 1.5 – 2.5%) in a mixture of O_2 and N_2O. After analgesia (Carprofen 5mg/kg i.p.) and disinfection, animals were fixed in a Kopf stereotax and injected into the scalp with a mix of lidocaine (6 mg/kg)/bupivacaine (2.5 mg/kg). To expose the skull, the skin was incised, and the bone scratched with a fresh scalpel blade to improve adhesion of the head implant. Then, we drilled small craniotomies (0.3 – 0.5 mm) over left frontal and parietal bones and positioned two conventional gold-coated copper-wire electrodes in contact with the dura mater for EEG recordings. In case of unilateral LC injections, EEG electrodes were implanted contralaterally. On the ipsilateral (right) side, high-impedance tungsten LFP microelectrodes (10–12 MΩ, 75-μm shaft diameter, FHC) were implanted in the primary somatosensory cortex (L +3.0; AP -0.7; D -0.85) and the hippocampus (L +2.0; AP -2.46; D -1.2 to -1.3). Additionally, as a neutral reference, a silver wire (Harvard Apparatus) was inserted into the occipital bone over the cerebellum and two gold pellets were inserted into the neck muscles for EMG recordings. All electrodes were fixed using Loctite Schnellkleber 401 glue and soldered to a multisite connector (Barrettes Connectors 1.27 mm, male connectors, Conrad). Animals were single housed after surgeries.

Surgeries for fiber photometry recordings. For fiber photometry, fiber implantation occurred together with the surgical implantations for sleep recordings. Shortly, an optic fiber stub coupled to a cannula (Doric Lenses, MFC_400/430-0.66_3.5mm_ZF1.25(G)_FLT) was implanted over the right LC (L +0.9; AP -5.4; D -2.7) at an insertion speed of 1 mm/min using a Kopf stereotaxic holder, for 1 animal the fiber was implanted with an angle of 20 degrees leading to a different set of coordinates (L +1.84; AP -5.4; D -2.9). For dual fiber photometry, this procedure was repeated over the primary somatosensory

thalamus (L +1.8; AP -1.7; D-2.5) over which the fiber stub was vertically inserted. Fibers were glued to the skull and were part of the dental cement structure holding the entire implant into place.

Surgeries for optogenetics. For optogenetic stimulation of noradrenergic LC neurons, 4 mm-long optic fibers were purchased pre-pared (MFC_200/250-0.66_4mm_ZF1.25(G)_FLT) or fabricated from a multimode fiber (225 μm outer diameter, Thorlabs, BFL37-2000/FT200EMT) using the custom-made procedure described in ref. [11]. For optogenetic inhibition 5 mm-long optic fibers attached to an optic canula were used (CFMLC12L05, Thorlabs). The implantation coordinates for stimulation were (L +0.9; AP -5.4; D -2.5 unilaterally in the right LC), while for inhibition two fibers were implanted bilaterally using a 20° angle from the vertical with coordinates (L +/-1.84; AP -5.4; D -2.5) from bregma. The emitted light intensity at the fiber tip was evaluated prior to implantation for every fiber.

RECORDING PROCEDURES AND PROTOCOLS

Sleep recordings. Sleep recordings always took place within the animals' home cage. Once recovered from surgery for > 1 week, animals were habituated to cabling to an ultrathin Intan SPI cable and adaptor board via a custom-made support system (Homemade adapters containing an Omnetics A79022-001 connector linked to a female Barrettes Connector from Conrad). These served as intermediate between the head implant of the animal and the headstage (RHD2132 amplifier board) that was connected to the Intan USB interface Acquisition Board (RHD2000). All signals (EEG frontal and parietal, left and right EMG, S1 and CA1 LFPs) were acquired in unipolar mode at 1 kHz.

All recordings were done in the 12-h light phase (ZT0-ZT12). For closed-loop optogenetic stimulation and inhibition, sessions timed to the infraslow σ power fluctuations in NREMS, 2 sessions were done per condition (Rising or declining σ power, Sham or Light stimulation). In experiments using optogenetic stimulation or inhibition according to the infraslow phase, sessions were spaced by one day. For optogenetic inhibition timed to the early or the late phase of the NREM-REMS cycle, 10 to 20 sessions per animal were recorded over 3 weeks' time. For the two REMS-R sessions per animal, at least 2 interleaved days were given. Per animal, there were 1-2 SDs that were kept at least 7 days

apart. The SSD was spaced apart from the SD sessions by at least 7 days. For details of the light exposure, see 'Optogenetic protocols'.

Fiber photometry recordings. Fiber photometry recording sessions took place at least one week after surgery and >1 day apart. Two signal generators modulated the blue (465 nm) and the violet (405 nm) LED of the Doric Fluorescence MiniCube LEDs (ilFMC4-G2_IE(400-410)_E(460-490)_F(500-550)_S) using sinusoidal signals at 319 and 211 Hz, respectively. The combined modulated light was then transmitted through a 400-µm-thick fiberoptic patchcord (MFP_400/430/1100-0.57_1m_FMC-ZF1.25_LAF, Doric Lenses) to the implanted optic canula on the head of the animal. A photodetector integrated into the MiniCube turned the emitted light from the fluorescent sensors into a current signal that was fed into an analog signal of the Intan RHD2132 amplifier board as described previously [11]. The measured power at the tip of the optic fiber was for both wavelengths between 20-30 µW ensuring minimal bleaching throughout the 12 hours of recordings.

Optogenetics protocols. For optogenetic interference at different phases of the infraslow σ power fluctuations, protocols were applied as described [11]. The optogenetic manipulations took place every first 20 min per hour from ZT1-ZT9. Stimulation sessions (with LED on) took place in exchange with sham session (LED off). Entries into NREMS were detected online through setting a threshold for the low-frequency (1 – 4 Hz) over θ (6 – 10 Hz) ratio for the differential frontal-parietal EEG signal and the decline in the absolute EMG amplitude. Occasional brief interruptions in LED stimulation during NREMS are due to a trespassing of that ratio, either caused by muscle twitches or spectral fluctuations. Once in NREMS, σ power fluctuations were monitored online and increasing or decreasing slopes detected through a machine-learning procedure [11]. For LC stimulation, we used 1 Hz pulses of 10 ms applied to a PlexBright Plexon BlueLED unit emitting 465 nm blue light at 2.8-3.2 mW intensity. For LC inhibition, we used continuous stimulation of an orange LED module (620 nm, 1.55 – 1.7 mW at the tip).

For optogenetic interference at different time points in the NREMS-REMS cycle, we used a closed-loop algorithm based on the low-frequency (1 – 4 Hz) over θ (6 – 10 Hz) ratio for the differential frontal-parietal EEG signal and the EMG activity on 4 s windows with a 3 s overlap (i.e. updated every second) to identify REM and NREM sleep as previously described [15]. Upon online identification of long REM bouts (>120 s), 20 min continuous optogenetic inhibition started randomly after 50 – 100 s of NREMS (*inhibition in refractory (Ref) period*), or after twice the time of the identified REM bout (= 240 s) with a random 10-s jitter (*inhibition in permissive (Perm) period*). Several sessions were recorded so that we collected around 10 episodes of long REM bouts per condition (Ref vs Perm).

For optogenetic inhibition after SSD (see below for procedure), LC was continuously inhibited for 1 or 2 h after the end of the SSD using continuous illumination. The stimulation started after a 10-s long NREMS was automatically detected, using a closed-loop algorithm based on the low-frequency (1 – 4 Hz) over θ (6 – 10 Hz) ratio for the differential frontal-parietal EEG signal and the EMG activity. Per animal, one SSD followed by LC inhibition and one SSD followed by Sham inhibition was carried out, with the SSDs spaced 2 weeks apart and inhibition or sham conditions were randomly assigned.

BEHAVIORAL MANIPULATIONS

REMS restriction (REMS-R). We used small vibrating motors (DC 3–4.2 V Button Type Vibration Motor, diameter 11 mm, thickness 3 mm) that we fixed using double-sided tape to the end of the recording cables, close to the animals' heads. The motors were driven to vibrate through a closed-loop system using a Raspberry Pi [15]. Once the θ (6 – 10 Hz) / δ (1 – 4 Hz) ratio of the CA1 LFP signal passed a threshold 1.5 for > 2 sec, the motors vibrated for 2 s and woke up the animal, as monitored by polysomnography. A control session for protocol standardization was included in which the motor of an animal was activated based on the closed-loop of the neighbor animal (yoked controls in Suppl. Fig. 4 a-c). The animals included only for the validation for the REMS-R procedure (Fig. 4 a,b and Suppl. Fig. 4) were separate from the ones in which LC activity was monitored or optogenetically altered during the REMS-R (Fig. 4c-g) in terms of analysis. The REMS-R was carried out from ZT0-ZT6 for all experiments except

when REMS-R was combined with LC optogenetic stimulation. Then, REMS-R lasted from ZT1-ZT9 and 20 min optogenetic stimulation was applied during NREM sleep once per hour as described above (optogenetic protocols).

Gentle sleep deprivation (SD). Animals were kept awake from ZT0-ZT4 while in their home cage and tethered to the recording apparatus. One person supervised two animals at the time and added nesting materials (pieces of Kleenex tissue) or gently interfered with the animals' spontaneous behavior once it started adopting a sleeping posture [42]. For this, we used an ~30 cm-long stick scotched to a ball of Kleenex tissue to gentle displace the litter around the nest or to wipe the wall of the cage. The animal was never touched throughout the entire procedure.

Stimulus-enriched sleep deprivation (SSD). The animals were placed in a novel cage and subjected to several manipulations every 20-30 min to touching (1-2 min), gentle cage shaking (5 min) or auditory stimulation (knocking at the cage, 5 min) from ZT0-ZT4. Two animals were supervised per person. These manipulations were paired one each for touching and cage shaking and auditory stimulation and cage shaking, and once done the three together. At the end, animals were transferred back to their home cage and left undisturbed. In animals used for fiber photometric recording of LC fluorescence, one SSD was carried out. In animals in which LC was inhibited after SSD, two SSDs per animal were carried out (one for sham inhibition, one for light inhibition). Corticosterone measures were carried out at ZT4 for baseline (undisturbed) and SSD conditions per animal by drawing tail vein blood samples. Samples were kept on ice in heparin-coated tubes and centrifuged at 4° for 4 min 9,400xg. Plasma was extracted and corticosterone levels measured with the Enzo Life Sciences kit (Catalog No. ADI-901-097).

HISTOLOGY

At the end of all the recording sessions the animal was injected i.p. with a lethal dose of pentobarbital. The position of each LFP electrode was subsequently marked using electro-coagulations (50 µA, 8 – 10 s). Afterwards, ~40 mL paraformaldehyde (4%) were perfused intracardially at a rate of ~3mL min^{-1}.

The brains were then extracted and post-fixed for at least 24 h in 4% PFA at 4 °C. Subsequently, the tissue was sliced in 50 µm-thick (for brainstem) or 100 µm-thick (for thalamus or cortex) sections using either a vibratome (Microtome Leica VT1000 S; speed: 0.25 – 0.5 mm s^{-1} and knife sectioning frequency: 65 Hz) or a freezing microtome (Microm). After cutting, the slices were either directly mounted (using Moviol as a mounting medium) or stored in 0.1M PB. Finally, we confirmed the anatomical location of the LFP and the viral-mediated expression of the fluorescent proteins with a Nikon SMZ25 Stereomicroscope equipped with a Nikon DS-Ri2 16 Mpx color camera. For a higher magnification image an Axiovision Imager Z1 (Zeiss) microscope was used (objectives used EC-Plan Neofluar 2.5x/0.075 ∞/0.17, 5x/0.16 ∞/0.17, 10x/0.3 ∞/- or 20x/0.5 ∞/0.17).

For immuno-amplification of the GFP signals, brain sections 50 µm-thick were first washed in 0.3% Triton in PBS 3 times. They were, then, incubated for 1 h in blocking solution of PBS 0.3% and 2% normal goat serum. Subsequently, they were incubated overnight with the primary antibody (monoclonal mouse anti-GFP, dilution 1:1000, Roche, 1 814 460) at 4 °C while on a shaker. After a total incubation for at least 12 h, the slices were washed 3 times with PBS containing 0.3% Triton. Afterwards, the secondary antibody was added (1:150 goat anti-mouse antibody coupled to Alexa Fluor 488, Invitrogene, A32723, in PBS containing 0.3% Triton) and the slices were incubated for 1-1.5 h at room temperature on a shaking platform. At the end of the procedure the slices were rinsed with PB 0.1 M and mounted (using again Moviol as a mounting solution).

ANALYSIS PROCEDURES

Sleep analysis.

Sleep scoring. We scored sleep stages in 4-s epoch using the EEG/EMG signals according to standard procedures using a custom-made semiautomated Matlab routine available on our Github Repository (https://github.com/Romain2-5/IntanLuthiLab). For every epoch, EEG was inspected for its spectral composition and the EMG for its level of activity. Wakefulness was scored when high-frequency phasic EEG activity coincided with strong EMG activity; NREMS was scored when high-amplitude low-

frequency components, such as slow oscillations (0.5 – 1.5 Hz) and δ activity (1.5 – 4 Hz), and recurrent sleep spindles (10 – 15 Hz) appeared in combination with low muscle tone; REMS was scored whenever a θ peak (6 – 10 Hz) appeared and muscle atonia developed. For determining the exact onset of REMS, a thresholding of θ/δ power was used for the CA1 LFP signal (see Spectral dynamics below). For epochs at transitions, the vigilance state that covered more than half of the epoch (> 2 s) was scored. Microarousals were scored when maximally 3 wake epochs (≤ 12 s) showing both EEG desynchronization (predominance of faster, low-amplitude, over slower high-amplitude activity) and EMG activity appeared sequentially and were both preceded and followed by NREMS. An epoch was also scored as MA when wake activity (in both EEG and EMG) lasted < 2 s. For analysis of intervals between successive REMS episodes during REMS-R, the motor vibration signal was used.

Spectral dynamics. The dynamics of spectral bands were calculated from the S1 and CA1 LFPs using wavelet transforms with Gabor-Morlet Kernels with 4 cycles of standard deviation for the Gaussian envelope at 0.1 Hz resolution. For spectral analysis involving S1 LFP signals or EEG, frequency bands analyzed were δ (1.5 – 4 Hz) , θ (6 – 10 Hz), σ (10 – 15 Hz), β (16 – 25 Hz), γ (60 – 80 Hz). For one analysis in Suppl Fig. 2, a division into low (26 – 40 Hz) and high γ (60 – 80 Hz) was made. The hippocampal LFP was used for calculation of the ratio of a θ (6 – 10 Hz) over δ (1 – 4 Hz) ratio (θ/δ) in the CA1 LFP electrode, in which the δ band was started at 1 Hz for convenience. For band-defined dynamic changes, the S1 or EEG signal were first down-sampled from 1 kHz to 200 Hz, the Wavelet transform calculated within the desired frequency bands and collapsing the frequency dimension. The derived signals were down-sampled at 10 Hz and low-pass-filtered at a cut-off frequency of 0.1 Hz. The detection of individual spindles was calculated as previously described [11,29]. For the CA1 signal, a similar procedure was applied to obtain the ratio for θ/δ and a threshold of 1.5 was chosen to define REMS onset around the previously defined manual transition. The dynamics of the EMG were calculated as absolute values from the 0.1 Hz-filtered trace.

Fiber photometric analysis.

Extraction of $\Delta F/F_0$ signals and baseline correction. Using the modulated recorded photometry signal, we demodulated two separate channels. A functional signal (from the blue excitation LED), carrying the calcium-dependent activity, and an isosbestic, calcium-independent one (from the violet excitation LED). We utilized the workflow and the MATLAB codes available as open-source[78]. Afterwards, the $\Delta F/F_0$ signal was computed using as F_0 the fitted isosbestic signal, following the procedure explained in [79].

For all analysis, fiber photometric signals were included in the analysis only if the dynamic range, calculated between the minimum and the maximum of the signal within the first 2 h of the recording, was > 15%. In the next paragraphs describing specific analyses, this extracted signal is referred to as the 'LC signal'.

Violin plot analysis of the LC signal. Violin plots were created through the DistributionPlot function from Jonas Dorn from the Mathworks file exchange [80] after selecting data points based on the 4-s epoch scoring for the first 2 h of the recordings. The z-scoring was calculated based on this selected dataset. Data for MAs were included in the distribution for waking. The occasional coexistence of vigilance states in 4-s epochs at transitional periods was not corrected for.

Peak detection and decay time analysis of the LC signal. For an initial unbiased analysis of peaks in the LC signal, we used the fluorescent signal low-pass-filtered at 0.5 Hz (see Suppl. Fig. 1). To calculate a lower envelope, a second filtered at 0.1 Hz was applied and the Envelope function of Matlab, (using a 96 s window) was used to obtain the lower envelope of the filtered signal. This envelope was then subtracted from the 0.5 Hz signal for baseline corrections. From the resulting timeseries, the FindPeaks function of Matlab was used to detect peak events within the upper 40% of prominence amongst peaks that had passed a threshold of 25% of the signal's dynamic range. For this peak analysis, MAs were included. For the peak analysis at Wake-to-NREMS transitions, LC signal and peaks were extracted from the transitions followed by >60 s of wake and a subsequent NREMS (including MAs) > 96 s. Time was normalized to study the decay of peak frequency in 11 bins. We additionally calculated the τ of the monoexponential fit of the filtered signal. For peak analysis after SD and SSD, mean peak frequency

values were calculated for equal times spent in NREMS (12 bins for baseline conditions, 8 for the SD and SSD conditions).

Cross-correlations between LC signals and σ power. Cross-correlations were calculated analogously to the previous one done for NA fluctuations and σ power [11] using z-scored σ power and LC signals at 0.1-s resolution for all NREMS bouts >96 s, including MAs, from ZT0-ZT12. A mean cross-correlation per animal was calculated and presented for the time interval between -200 s to 200 s, from which the position of side peaks could be extracted in 6 out of 8 cases (based on the dynamic range of the LC signal). Cross-correlations were then averaged across animals. A positive time lag indicates that the LC signal increases preceded σ power decreases. We refer to 'LC transients' as the LC activity peaks that anticorrelate with the σ power.

Spectral analysis of LC peaks. Local maxima of the LC signals were defined using a 20-s sliding window on the LC $\Delta F/F_0$ signal. We then derived the z-scored spectral dynamics for different frequency bands using the wavelet approached previously described (See *Sleep Analysis - Spectral dynamics*) around these maxima from – 50 s to + 50 s. In a second step, these peaks were classified according to whether or not they were associated with a short MA (< 4 s) or a long MA (> 4 s) (defined by EEG/EMG activity as described in *Sleep Analysis – Sleep Scoring*) within 5 s around the peak. This analysis was carried out both for the S1 LFP signal and for the EEG during NREMS bouts for all times excluding the ones falling within the initial monoexponential decay (see *Fiber photometric analysis - Peak detection and decay time analysis of the LC signal*). In a supplementary analysis, we further subdivided MA into short (< 4 s), intermediate (> 4 s, < 8 s) and long (> 8 s). Mean values for the LC signal were calculated from times 0 s to 5 s and averaged.

Spectral analysis at REMS onset. The exact timing of REMS onset was defined using a thresholding for θ/δ at 1.5 using the CA1 LFP electrode. Using the parietal EEG electrode provided similar time points. The dynamics for preceding NREMS were then obtained for the S1 LFP σ band and for the low-pass filtered absolute EMG signal. For LC signals with high dynamic range, an inflection point could be observed prior to REMS onset after which there was a further decrease to a new minimum (see e.g.

Fig. 2c). This inflection point was associated with a further increase in σ power and the onset of EMG decline, consistent with markers for 'Intermediate sleep'.

Sleep architecture analysis during LC optogenetic stimulation and inhibition. For LC stimulation or inhibition according to the phase of the σ power fluctuation, times spent in Wake, NREMS and REMS were calculated for the test or sham stimulation 20-min sessions and expressed in % of total time. Transitions were calculated as the number of REMS-epochs followed by NREMS. For LC inhibition at different moments in the NREMS-REMS cycle, a similar procedure was applied.

Mean LC activity in NREMS bouts. The LC fluorescent signal was extracted between REMS bouts lasting ≥ 12 s, z-scored for all NREMS including MAs, and plotted over normalized NREM time between the consecutive REM bouts. The derived signals were averaged based on the length of the preceding REM bout as previously done for similar purposes [39].

Quantification of rebound REMS after REMS-R. To demonstrate the efficiency of the REMS-R, we also quantified rebound REMS by calculating cumulative times spent in REMS during REMS-R and the 6 h – post REMS-R period.

LC signal analysis during REMS-R. To determine the relative level of LC activity prior to REMS entry during the REMS-R, we extracted bouts where a transition to REMS was present and preceded by at least 12 sec of NREM sleep. The $\Delta F/F_0$ LC activity was then z-scored for each bout and the minimum activity was defined as the mean $\Delta F/F_0$ value during the last 5 sec before the transition to REMS.

LC stimulation during REMS-R. For each 20 min stimulation block (first 20 min of every hour from ZT1–ZT9) during the REMS-R, we normalized the time in equal amounts of NREMS for the periods before, during and after stimulation (10 bins per block) and calculated the number of REM entries per min of NREMS. A similar approach was done to the analogous periods during sham stimulation, *ceteris paribus*, with the LEDs turned off.

STATISTICS

The statistics were done using Python, Matlab R2021a or R statistical language version 4.0.1. The normality of data distributions were assessed using the Shapiro–Wilk and Levene tests to decide for parametric statistics. In the cases where normality was violated, a non-parametric Kruskal-Wallis instead of ANOVAs were used. Datasets were collected in experimental designs allowing preferentially repeated measures and/or paired statistical analysis. Post-hoc analyses were done only when the one-way factor or the interaction between factors was significant ($p<0.05$). Bonferroni's correction for multiple comparisons was applied routinely, and the corrected α thresholds are given in the Supplementary Table 1 summarizing all statistical results. In the legends, only the statistical tests are given, and the number of samples and the p values are indicated in the figures.